X-ray Structural Determination of Complex 5. The diffraction intensities of an approximately 0.3 × 0.3 × 0.3 mm crystal were collected with graphite monochromatized Cu Kα radiation with the $\theta/2\theta$ scan technique and profile analysis to $2\theta_{max} = 120°$.[16] A total of 1498 unique reflections were measured, of which 1075 were considered significant with $I_{net} > 2.5\sigma(I_{net})$. Lorentz and polarization factors were applied, and absorption corrections were made ($u = 7.25$ mm^{-1}). The minimum transmission coefficient was 0.3150 while the maximum value is 0.4316. The cell parameters were obtained by least-squares refinement of the setting angles of 50 reflections with $2\theta > 120°$ (λ(Cu Kα_1) = 1.54056 Å). The structure was solved by MULTAN,[19] and H atom positions were calculated. The structure was refined by full-matrix least-squares methods to final residuals of $R_F = 0.042$ and $R_{wF} = 0.049$ for the significant data ($R_F = 0.059$ and $R_{wF} = 0.051$ for all data) with counting statistics weights. The final atomic positional parameters and the equivalent isotropic thermal factors are listed in Table VIII. Other details of the refinement were as described for complex **1**.

Acknowledgment. We are grateful to the donors of the Petroleum Research Fund, administered by the American Chemical Society, for financial support. We also thank the National Science Foundation for an instrument grant toward the purchase of the FT-NMR spectrometer.

Supplementary Material Available: Tables of bond angles and distances and isotropic and anisotropic thermal parameters for **1** and **5** (5 pages); tables of observed and calculated structure factors (34 pages). Ordering information is given on any current masthead page.

C-H Oxidative Addition and Reductive Elimination Reactions in a Dinuclear Iridium Complex

William D. McGhee, Frederick J. Hollander, and Robert G. Bergman*

Contribution from the Materials and Chemical Sciences Division, Lawrence Berkeley Laboratory, 1 Cyclotron Road, and the Department of Chemistry, University of California, Berkeley, California 94720. *Received February 5, 1988*

Abstract: Thermolysis of the hydridoallyliridium complex (η^5-C_5Me_5)(η^3-C_3H_5)(H)Ir at relatively high concentrations of starting material in benzene leads to the dinuclear benzene C-H oxidative addition product (η^5-C_5Me_5)(C_6H_5)Ir(η^1,η^3-C_3H_4)(μ-H)-Ir(η^5-C_5Me_5) (**1**). Heating this material causes reductive elimination of benzene from the dinuclear complex **1** in a clean first-order process. The lack of dependence of the rate of this process on the concentration of entering ligand demonstrates that an intermediate is formed in the reductive elimination; this species is proposed to be the coordinatively unsaturated dinuclear complex (η^5-C_5Me_5)Ir(η^1,η^3-C_3H_4)Ir(η^5-C_5Me_5) (**13**). Transient intermediate **13** reacts with dative ligands such as phosphines, ethylene, and *tert*-butyl isocyanide to give direct trapping products (η^5-C_5Me_5)(L)Ir(η^1,η^3-C_3H_4)Ir(η^5-C_5Me_5) (**2**-**6**), formed by coordination of the ligand to one of the iridium centers. Reaction of **13** with reagents having activated X-H bonds, such as benzene-d_6, H_2, and acetonitrile, leads to intermolecular oxidative addition products having structures analogous to that of **1**. Comparative inter- and intramolecular kinetic isotope effect studies have provided evidence that in the reversible reaction of **13** with benzene, an additional η^2-arene intermediate is not required to explain the results. Thermolysis of **2** and **4**, the PMe_3- and ethylene-trapped products of **13**, leads to three new dinuclear complexes (**7**, **8**, and **9**). These materials are formed by intramolecular insertion into the dative ligand C-H bonds, followed by rearrangement. The structures of the intermolecular benzene C-H insertion product **1**, PMe_3-trapped product **2**, and intramolecular C-H activation product **7** have been determined by X-ray diffraction.

There are now several examples of homogeneous intermolecular carbon-hydrogen bond activation at transition-metal centers.[1] In most of these cases, complexes with only one metal center are used. In the few systems reported in which more than one metal center is present in the reacting complex, little is known about the mechanism of the process in which the C-H bond is cleaved.[2] The reverse reaction, reductive elimination giving a newly formed C-H bond, finds ample precedent in mononuclear systems;[3] however, multinuclear reductive eliminations are still rare.[4] The two most extensively studied systems are those reported by Norton and Stille. In Norton's account the intervention of a bridging metal hydride prior to reductive elimination is discussed,[4b] while Stille proposed a rearrangement to an intermediate that has both the alkyl and

Scheme I

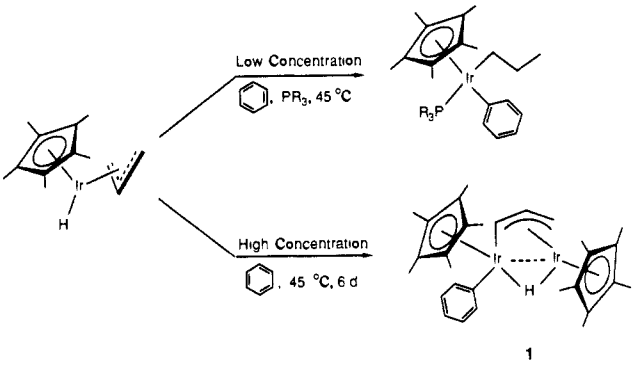

1

(1) For reviews see: (a) Parshll, G. W. *Acc. Chem. Res.* **1975**, *8*, 113. (b) Parshall, G. W. *Catalysis*; Kemball, C., Ed.; The Chemical Society: London, 1977; Specialist Periodical Reports, Vol. 1, p 335. (c) Muetterties, E. L. *Chem. Soc. Rev.* **1982**, *11*, 283. (d) Halpern, J. *Inorg. Chim. Acta* **1985**, *100*, 41. (e) Shilov, A. E. *Activation of Saturated Hydrocarbons Using Transition Metal Complexes*; D. Riedel: Dordrecht, 1984. (f) Crabtree, R. H. *Chem. Rev.* **1985**, *85*, 245. (g) Bergman, R. G. *Science (Washington, D.C.)* **1984**, *223*, 902.

(2) See, for example: (a) Berry, D. H.; Eisenberg, R. *J. Am. Chem. Soc.* **1985**, *107*, 7181. (b) Nubel, P. O.; Brown, T. L. *J. Am. Chem. Soc.* **1984**, *106*, 644. (c) *Ibid.* **1984**, *86*, 644. (d) Fryzuk, M. D.; Jones, T.; Einstein, F. W. B. *Organometallics* **1984**, *3*, 185 and reference cited there. (e) Bandy, J. A.; Cloke, F. G. N.; Green, M. L. H.; O'Hare, D.; Prout, K. *J. Chem. Soc., Chem. Commun.* **1984**, 240. (f) Green, M. L. H.; O'Hare, D.; Bandy, J. A.; Prout, K. *Ibid.* **1984**, *884*. (g) Cloke, F. G. N.; Derome, A. E.; Green, M. L. H.; O'Hare, D. *Ibid.* **1983**, 1312.

(3) For a review see: Halpern, J. *Acc. Chem. Res.* **1982**, *15*, 332.

(4) (a) Kellenburger, B.; Young, S. J.; Stille, J. K. *J. Am. Chem. Soc.* **1985**, *107*, 6105. (b) Carter, W. J.; Okrasinski, S. J.; Norton, J. R. *Organometallics* **1985**, *4*, 1376. For a theoretical analysis see: Trinquler, G.; Hoffmann, R. *Organometallics* **1984**, *3*, 370.

0002-7863/88/1510-8428$01.50/0

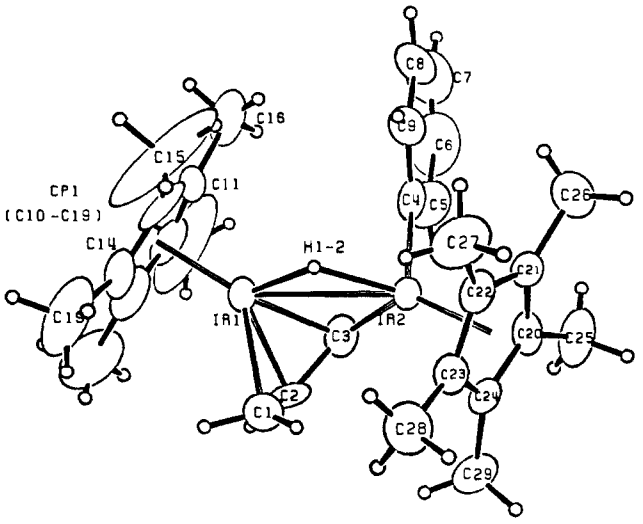

Figure 1. ORTEP diagram of one of the molecules of **1**.

hydride ligand on the same metal center.[4a] The pathway leading to this intermediate may also contain a species with a bridging metal hydride.

While studying the chemistry of $(\eta^5\text{-}C_5Me_5)Ir(\eta^3\text{-}C_3H_5)H$,[5a,b] we uncovered the synthesis of dinuclear hydridophenyliridium complex **1** (shown in Scheme I), which resembles the intermediate bridging hydride species suggested by Norton. This account describes the reductive elimination of benzene from **1** and a study of the mechanism of this reaction. The formal oxidative addition of a C–H bond of benzene across an Ir–Ir single bond is also reported, as well as other inter- and intramolecular C–H bond cleavage reactions.[5c]

Results

Chemistry of $(\eta^5\text{-}C_5Me_5)(C_6H_5)Ir(\eta^1,\eta^3\text{-}C_3H_4)(\mu\text{-}H)Ir(\eta^5\text{-}C_5Me_5)$ (1). Synthesis and Solid-State Structure. Reaction of dilute benzene solutions of $(\eta^5\text{-}C_5Me_5)Ir(\eta^3\text{-}C_3H_5)H$ with phosphines leads to $(\eta^5\text{-}C_5Me_5)(PR_3)Ir(Ph)(n\text{-}Pr)$, as has been described earlier[5b] (Scheme I). However, thermolysis at higher concentrations (ca. 0.5–1.0 M) of the allyl hydride in the absence of phosphine takes a different course, leading typically to 60% yields of **1** as red-orange crystals (presumably with loss of propene and H_2). This new dinuclear complex is air stable in the solid state while solutions decompose over the course of a few hours; the complex is stable indefinitely at room temperature under nitrogen. The mild reaction conditions used for the synthesis of **1** are necessary as higher reaction temperatures give rise to substantially lower isolated yields.

This new complex can be assigned spectroscopically as the structure shown in Scheme I, $(\eta^5\text{-}C_5Me_5)(C_6H_5)Ir(\mu\text{-}H)(\eta^1,\eta^3\text{-}C_3H_4)Ir(\eta^5\text{-}C_5Me_5)$. In the ^1H NMR spectrum the η^1,η^3-allyl ligand is easily distinguished from the normal $\eta^3\text{-}C_3H_5$ ligand by the downfield resonance, corresponding to the α-CH proton, at δ 7.78 ppm (d, J = 5.4 Hz).[6] This type of ligation is also evident in the ^{13}C NMR spectrum where the resonances for the allyl carbons appear at δ 105.8 (d, J = 154.3 Hz), 84.2 (d, J = 156.1 Hz), and 30.99 ppm (t, J = 155 Hz). In the ^1H NMR spectrum the iridium hydride resonance at δ −20.48 ppm is substantially upfield of that for Ir–H in $(\eta^5\text{-}C_5Me_5)Ir(\eta^3\text{-}C_3H_5)H$, δ −16.7 ppm.[5] This type of upfield shift is consistent with, but not conclusive proof of, a bridging metal–hydride linkage.[7] In support of this assignment is the absence of an Ir–H stretch in the solid-state IR spectrum in the range 2400–1600 cm^{-1}, which is the typical range for terminal metal hydrides.[8] The exact pathway for the formation of **1** is not known; however, it is clear that both a C–H bond in a $(\eta^3\text{-}C_3H_5)$ ligand and a C–H bond in benzene are cleaved. The formation of a η^1,η^3-allyl ligand from an η^3-allyl moiety has been reported previously.[9]

Scheme II

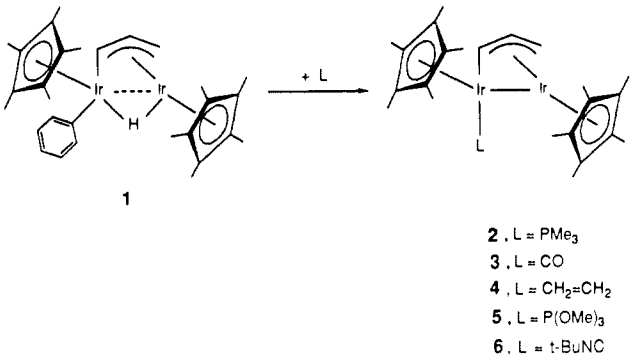

To establish the exact nature of the bonding in **1**, a single-crystal X-ray structure determination was performed. Suitable crystals for the determination were grown by slow cooling of a toluene/hexane solution giving red-orange, block-like crystals. An ORTEP diagram of one of the molecules in the asymmetric unit of **1** is shown in Figure 1 and bond distances and angles are given in Tables I and II; other data are given in the Experimental Section and supplementary material to the preliminary communication.[5c] The structure clearly shows the η^1,η^3-allyl linkage with Ir–C3 distances of 2.160 (6) and 2.007 (7) Å and nearly equivalent C–C distances of 1.41 (1) and 1.43 (1) Å. This implies that the bonding is more consistent with the η^1,η^3-allyl formulation than a μ-CH-η^2-CH=CH_2 type of structure.[10] Several X-ray structures containing the η^1,η^3-allyl ligand have been reported and the bonding in **1** is unexceptional.[11] The hydride was located by difference Fourier techniques; in the solid state it clearly bridges the two iridium centers with Ir–H distances of 1.74 (6) and 1.78 (6) Å. The iridium–iridium distance of 2.867 (1) Å is within bonding distance, consistent with a hydrogen-bridged metal–metal bond between the two iridium atom centers and the hydride.[12] It is also evident from the structure that the phenyl group is σ-bound to only one iridium atom and is outside normal bonding

(5) (a) McGhee, W. D.; Bergman, R. G. *J. Am. Chem. Soc.* **1985**, *107*, 3388. (b) McGhee, W. D.; Bergman, R. G. *J. Am. Chem. Soc.* **1988**, *110*, 4246. (c) Portions of this work have been reported earlier in preliminary form: McGhee, W. D.; Bergman, R. G. *J. Am. Chem. Soc.* **1986**, *108*, 5621.

(6) The $(\eta^3\text{-}C_3H_5)$ ligand in several iridium complexes has, typically, proton resonances at δ 3.5–2.8 ppm for the β-proton and δ 3–1 ppm for the α-proton: see ref 5.

(7) A recent discussion on this topic appears in: Legzdins, P.; Martin, J. T.; Einstein, W. B.; Willis, A. C. *J. Am. Chem. Soc.* **1986**, *108*, 7971.

(8) Muetterties, E. L., Ed. *Transition Metal Hydrides*; Marcel Dekker, Inc.: New York, 1971.

(9) Eisenstadt, A.; Efraty, A. *Organometallics* **1982**, *1*, 1100.

(10) A discussion of possible isomers of the η^1,η^3-allyl ligand appears in ref 11p.

(11) (a) Parlier, A.; Rudler, M.; Rudler, H.; Daran, J. C. *J. Organomet. Chem.* **1987**, *323*, 353. (b) Brammer, L.; Green, M.; Orpen, A. G.; Paddick, K. E.; Saunders, D. R. *J. Chem. Soc., Dalton* **1986**, 657. (c) Jeffery, J. C.; Moore, I.; Razay, H.; Stone, F. G. A. *J. Chem. Soc., Dalton* **1984**, 1581. (d) Jeffery, J. C.; Moore, I.; Stone, F. G. A. *Ibid.* **1984**, 1571. (e) Jeffery, J. C.; Laurie, J. C. V.; Moore, I.; Razay, H.; Stone, F. G. A. *Ibid.* **1984**, 1563. (f) Green, M.; Orpen, A. G.; Schaverien, C. J.; Williams, I. D. *J. Chem. Soc., Chem. Commun.* **1983**, 583. (g) King, J. A.; Vollhardt, K. P. C. *J. Am. Chem. Soc.* **1983**, *105*, 4846. (h) Green, M.; Orpen, A. G.; Schaverien, C. J.; Williams, I. D. *J. Chem. Soc., Chem. Commun.* **1983**, 1399. (i) Bott, S. G.; Connelly, N. G.; Green, M.; Norman, N. C.; Orpen, A. G.; Paxton, J. F.; Schaverien, C. J. *Ibid.* **1983**, 378. (j) Adams, P. Q.; Davies, D. L.; Dyke, A. F.; Knox, S. A. R.; Mead, K. A.; Woodward, P. *Ibid.* **1983**, 222. (k) Rudler, H.; Rose, R.; Rudler, M.; Alvarez, C. *J. Mol. Catal.* **1982**, *15*, 81. (l) Colbern, R. E.; Dyke, A. F.; Knox, S. A. R.; MacPherson, K. A.; Orpen, A. G. *J. Organomet. Chem.* **1982**, *239*, C15. (m) Muller, J.; Passon, B.; Pickardt, J. *J. Organomet. Chem.* **1982**, *236*, C11. (n) Green, M.; Norman, N. C.; Orpen, A. G. *J. Am. Chem. Soc.* **1981**, *103*, 1269. (o) Levisalles, J.; Rose-Munch, F.; Rudler H.; Daran, J.; Dormzee, Y.; Jeannin, Y.; Ades, D.; Fontanille, M. *J. Chem. Soc., Chem. Commun.* **1981**, 1055. (p) Dyke, A. F.; Guerchais, J. E.; Knox, S. A. R.; Rove, J.; Short, R. L.; Taylor, G. E.; Woodward, P. *Ibid.* **1981**, 537. (q) Levisalles, J.; Rose-Munch, F.; Rudler, H. *Ibid.* **1981**, 152. (r) Levisalles, J.; Rudler, H.; Dahan, F.; Jeannin, Y. *J. Organomet. Chem.* **1980**, *188*, 803. (s) Johnson, B. F. G.; Kelland, J. W.; Lewis, J.; Mann, A. L.; Raithby, P. R. *J. Chem. Soc., Chem. Commun.* **1980**, 547. (t) Dyke, A. F.; Knox, S. A. R.; Naish, P. J.; Taylor, G. E. *Ibid.* **1980**, 803. (u) Barker, G.; Carroll, W. D.; Green, M.; Welch, A. J. *Ibid.* **1980**, 1071.

(12) A discussion of the bonding in transition-metal three-center two-electron systems containing a bridging metal hydride appears in: Bau, R.; Teller, R. G.; Kirtley, S. W.; Koetzle, T. F. *Acc. Chem. Res.* **1979**, *12*, 179.

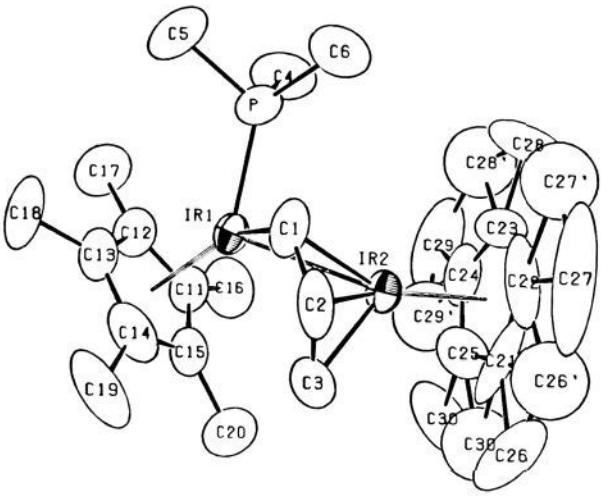

Figure 2. ORTEP diagram of **2**.

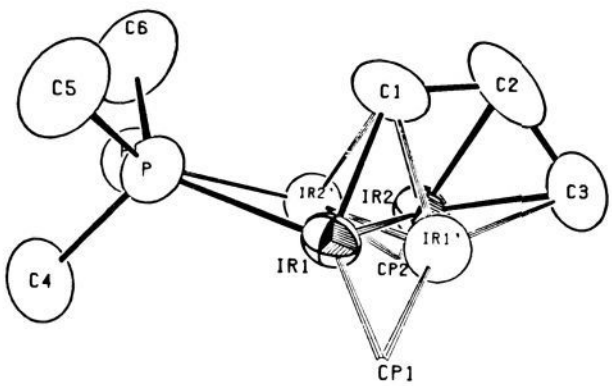

Figure 3. Partial ORTEP diagram of **2**, showing the disorder in the molecule.

distance to the bridging hydride.

Dinuclear Reductive Elimination of Benzene from 1: Synthesis and Solid-State Structure of (η^5-C_5Me_5)(PMe_3)Ir(η^1,η^3-C_3H_4)-Ir(η^5-C_5Me_5) (2). Addition of PMe_3 to a benzene or hexane solution of **1** followed by heating to 45 °C for 14 h did not convert it to (η^5-C_5Me_5)(PMe_3)Ir(Ph)(*n*-Pr), demonstrating that dinuclear complex **1** is not an intermediate in the earlier reported reaction of the allyl hydride with phosphines.[5] Instead, the reaction produced red crystals of a new dinuclear complex in 70% yield (Scheme II). Monitoring the reaction by ^{1}H NMR (C_6D_{12}) spectrometry showed the clean formation of this material, along with the production of 1 equiv of C_6H_6. The new complex was formulated as (η^5-C_5Me_5)(PMe_3)Ir(η^1,η^3-C_3H_4)Ir(η^5-C_5Me_5) (**2**, Scheme II) by standard analytical and spectroscopic techniques. In the ^{1}H NMR (C_6D_6) spectrum the metal-bound PMe_3 ligand appears at δ 1.34 ppm (d, J_{HP} = 9.3 Hz) and the α-CH proton of the η^1,η^3-allyl at δ 7.94 ppm (dd, J_{HH} = 5.1 Hz, J_{HP} = 16.7 Hz). In the ^{13}C NMR (C_6D_6) spectrum the carbon resonances for the η^1,η^3-allyl ligand appear at δ 107.7 (dd, J_{CH} = 151 Hz, J_{CP} = 9.5 Hz), 76.8 (d, J_{CH} = 158 Hz), and 29.5 ppm (t, J_{CH} = 151 Hz). Of particular note is the strong absorbance in the visible region of the UV–visible spectrum of **2**, $\lambda_{max} \approx 500$ nm ($\epsilon = 4.2 \times 10^3$). This value is comparable to the weaker absorbance at λ_{max} = 450 (ϵ = 650) in the spectrum of **1**. Because the conversion of **1** to **2** causes a formal reduction of each metal center (Ir^{III} to Ir^{II}), we decided to confirm the structure of **2** by X-ray diffraction.

Deep red crystals of **2** were grown by slow evaporation of diethyl ether from a solution of diethyl ether/acetonitrile at room temperature in the drybox. An ORTEP diagram for **2** is shown in Figures 2 and 3 with bond distances and angles given in Tables III and IV. Additional details of the diffraction study are provided in the Experimental Section and supplementary material. The

Scheme III

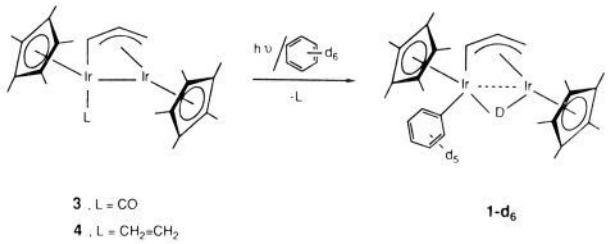

Scheme IV

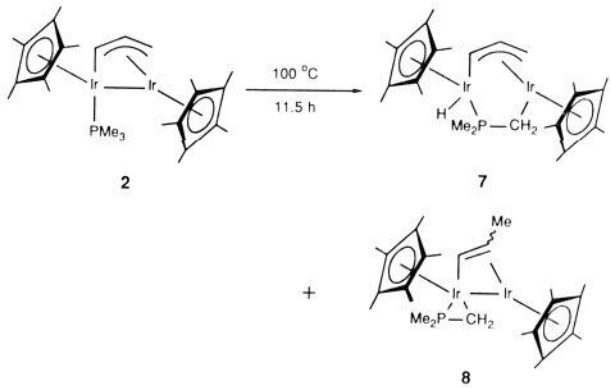

shortening of the iridium–iridium bond distance from 2.867 Å in **1** to 2.78 Å in **2** is presumably the result of the change from a hydrogen-bridged metal–metal bond to a direct metal–metal interaction. No chemically significant difference in the distances between the metal centers and the carbons of the η^1,η^3-allyl ligand are observed in the structures of **1** and **2**.

To test the generality of the reductive elimination of benzene we explored the reaction between **1** and several different donor ligands. The use of CO, ethylene, *t*-BuNC, and $P(OCH_3)_3$ produced complexes **3**–**6** (Scheme II), similar to the one observed utilizing PMe_3 (see Experimental Section for analytical and spectroscopic details). The λ_{max} in the UV–vis spectra for the d–d* transition in the complexes **2**–**6** progressively decreased following the order PMe_3 > $P(OCH_3)_3$ > ethylene > *t*-BuNC > CO. The weaker donor ligands THF, $N(Me_3)$, and pyridine did not react with **1** under the thermolysis conditions described above.

Irradiation of the Ethylene and CO Complexes 3 and 4 in Benzene. A well-documented method for inducing ligand loss followed by C–H bond oxidative addition is that of photoinduced ligand dissociation.[13] Both carbon monoxide and ethylene have been shown to undergo photodissociation from iridium complexes;[14] therefore, we investigated the photochemistry of complexes **3** and **4** in benzene. In both instances irradiation of benzene-d_6 solutions regenerated the benzene insertion product (in this case **1**-d_6), in 53–60% yields from CO complex **3** and 40–53% yields from ethylene complex **4** (Scheme III). Presumably, in each case irradiation causes ligand dissociation giving rise to a common unsaturated intermediate that is then capable of insertion into the C–D bond of benzene-d_6. Attempts at a similar reaction with pentane were unsuccessful, giving only intractable materials.

Thermolysis of CO, PMe_3, and Ethylene Complexes 3, 2, and 4. In contrast to its photochemistry, thermolysis of the CO complex **3** in benzene gave no reaction up to 165 °C. Heating either the PMe_3 complex **2** or the ethylene complex **4** gave no observable reaction with solvent by ^{1}H NMR spectroscopy.

(13) A general discussion of inorganic photochemistry appears in: (a) Adamson, A. W.; Fleischauer, P. D. *Concepts of Inorganic Photochemistry*; Wiley: New York, 1975. (b) Wrighton, M. S., Ed., *Inorganic and Organometallic Chemistry*; American Chemical Society: Washington, D.C., 1978; *ACS Adv. Chem Ser. No. 168.*

(14) (a) Hoyano, J. K.; Graham, W. A. G. *J. Am. Chem. Soc.* **1982**, *104*, 3723. (b) Hoyano, J. K.; McMaster, A. D.; Graham, W. A. G. *J. Am. Chem. Soc.* **1983**, *105*, 7190. (c) Haddleton, D. M.; Perutz, R. N. *J. Chem. Soc., Chem. Commun.* **1986**, 1734.

Table I. Selected Bond Distances for Complex 1

ATOM 1	ATOM 2	DISTANCE	ATOM 1	ATOM 2	DISTANCE
IR1	IR2	2.867(1)	IR3	IR4	2.872(1)
IR1	H1-2	1.74(6)	IR3	H3-4	1.80(5)
IR2	H1-2	1.78(6)	IR4	H3-4	1.72(6)
IR1	C1	2.132(8)	IR3	C31	2.132(6)
IR1	C2	2.144(7)	IR3	C32	2.118(5)
IR1	C3	2.160(6)	IR3	C33	2.166(5)
IR2	C3	2.007(7)	IR4	C33	2.015(6)
IR2	C4	2.035(6)	IR4	C34	2.033(6)
IR1	C10	2.162(6)	IR3	C40	2.215(5)
IR1	C11	2.239(7)	IR3	C41	2.216(6)
IR1	C12	2.198(6)	IR3	C42	2.251(6)
IR1	C13	2.141(7)	IR3	C43	2.175(6)
IR1	C14	2.170(6)	IR3	C44	2.159(6)
IR1	CP1	1.831	IR3	CP3	1.839
IR2	C20	2.149(6)	IR4	C50	2.147(6)
IR2	C21	2.230(6)	IR4	C51	2.215(6)
IR2	C22	2.258(5)	IR4	C52	2.247(6)
IR2	C23	2.300(6)	IR4	C53	2.286(6)
IR2	C24	2.241(6)	IR4	C54	2.255(5)
IR2	CP2	1.879	IR4	CP4	1.875
C1	C2	1.405(12)	C31	C32	1.414(9)
C2	C3	1.434(10)	C32	C33	1.409(9)
C4	C5	1.413(9)	C34	C35	1.402(8)
C4	C9	1.397(9)	C34	C39	1.405(9)
C5	C6	1.386(12)	C35	C36	1.376(10)
C6	C7	1.334(14)	C36	C37	1.371(11)
C7	C8	1.396(13)	C37	C38	1.397(10)
C8	C9	1.400(11)	C38	C39	1.400(10)
C10	C11	1.501(11)	C40	C41	1.428(9)
C11	C12	1.395(11)	C41	C42	1.428(8)
C12	C13	1.310(11)	C42	C43	1.393(9)
C13	C14	1.378(10)	C43	C44	1.452(8)
C14	C10	1.401(11)	C44	C40	1.430(8)
C10	C15	1.488(10)	C40	C45	1.510(8)
C11	C16	1.425(13)	C41	C46	1.488(9)
C12	C17	1.531(11)	C42	C47	1.493(9)
C13	C18	1.513(12)	C43	C48	1.509(9)
C14	C19	1.499(11)	C44	C49	1.479(9)
C20	C21	1.449(8)	C50	C51	1.442(9)
C21	C22	1.402(9)	C51	C52	1.397(9)
C22	C23	1.450(9)	C52	C53	1.434(9)
C23	C24	1.420(8)	C53	C54	1.406(8)
C24	C20	1.423(9)	C54	C50	1.428(8)
C20	C25	1.504(9)	C50	C55	1.498(8)
C21	C26	1.493(10)	C51	C56	1.483(10)
C22	C27	1.500(8)	C52	C57	1.511(9)
C23	C28	1.496(9)	C53	C58	1.496(10)
C24	C29	1.500(9)	C54	C59	1.495(9)

However, intramolecular C–H bond activation did occur in both cases. Thus, heating a solution of **2** to 100 °C for 11.5 h in benzene led to the formation of two new organometallic complexes in a 10:1 ratio (Scheme IV). During the course of the reaction the solution turned from deep red to light orange. The major product was isolated in 52% yield as light yellow crystals. The minor complex was identified by its characteristic ^1H NMR and $^{31}P\{^1H\}$ NMR spectra as structure **8** (vida infra). Spectroscopically the structure of the major product is consistent with **7**, shown in Scheme IV.[15] In the ^1H NMR spectrum the η^1,η^3-allyl ligand exhibits proton resonances at δ 4.46 (d, J = 7.1 Hz), 4.01 (q, J = 7.2 Hz), 2.63 (d, J = 5.7 Hz), and 1.81 (d, J = 8.9 Hz). It is interesting that the α-CH resonance appears substantially upfield (δ 4.46 ppm) from the other α-CH resonances observed in the η^1,η^3-allyl complexes described in this account (δ 7.12–8.21 ppm). The bridging phosphine ligand shows methyl proton resonances at δ 1.63 (d, J_{HP} = 8.6 Hz) and 1.12 (d, J_{HP} = 9.8 Hz) while the methylene protons appear at δ 2.47 (t, $J_{HH(gem)}$ = 11.3 Hz) and 1.45 ppm (dd, $J_{HH(gem)}$ = 11.3 Hz, J_{HP} = 4.8 Hz), clearly showing cleavage of a C–H bond in one of the methyl groups of the trimethylphosphine ligand. The iridium-bound hydride resonates at δ −18.1 ppm (d, J_{HP} = 37.7 Hz); the magnitude of the proton–phosphorus coupling constant implies that the hydride resides on an iridium center that also has a phosphorus atom bound to it. In support of a terminal hydride linkage is the appearance of a strong absorbance in the solid-state IR at 2120 cm^{-1}. The ^{13}C NMR spectrum also supports the structure shown for **7**. The η^1,η^3-allyl carbons appear at δ 82.4 (d, J_{CH} = 153.3 Hz), 42.4 (br d, J_{CH} = 136.5 Hz) 39.0 (t, J_{CH} = 153.7 Hz) ppm while the carbons in the bridging Me_2P–CH_2 ligand appear at δ 20.8 (dq, J_{CP} = 24.5 Hz, J_{CH} = 126.2 Hz), 18.26 (dt, J_{CP} = 33.4 Hz, J_{CH} = 125.6 Hz), and 15.21 ppm (dq, J_{CP} = 31.8 Hz, J_{CH} = 123 Hz). The $^{31}P\{^1H\}$ NMR resonance for this complex, δ 35.1 ppm, is very distinct, showing a large downfield shift from the resonance observed in complex **2** (δ −39.4 ppm).[16] The UV–visible spectrum for **7** (λ_{max} = 270, ϵ = 8 × 10^3, large tail out to ca. 375 nm) is strikingly different from that of complex **2** (λ_{max} = 276, ϵ = 1.6

(15) For examples of other complexes with the μ-η^2-CH_2PMe_2 ligand see: Wenzel, T. T.; Bergman, R. G. *J. Am. Chem. Soc.* **1986**, *108*, 4856 and references cited there.

(16) In ref 15 the $^{31}P\{^1H\}$ NMR spectrum exhibits this same downfield shift for the μ-η^2-CH_2PMe_2 ligand.

Table II. Selected Bond Angles for Complex 1

ATOM 1	ATOM 2	ATOM 3	ANGLE	ATOM 1	ATOM 2	ATOM 3	ANGLE
C11	C10	C14	105.7(6)	CP1	1R1	1R2	147.7
C10	C11	C12	103.3(7)	CP1	1R1	C1	132.9
C11	C12	C13	112.4(7)	CP1	1R1	C2	133.7
C12	C13	C14	110.0(8)	CP1	1R1	C3	140.0
C10	C14	C13	108.4(7)	CP1	1R1	H1-2	124.7
C11	C10	C15	125.9(12)	C1	1R1	H1-2	89.5(22)
C14	C10	C15	127.7(12)	C2	1R1	H1-2	101.6(21)
C10	C11	C16	130.1(12)	C3	1R1	H1-2	80.1(21)
C12	C11	C16	126.3(12)				
C11	C12	C17	123.1(11)	CP2	1R2	1R1	144.6
C13	C12	C17	124.5(10)	CP2	1R2	C3	134.1
C12	C13	C18	126.9(10)	CP2	1R2	C4	124.1
C14	C13	C18	122.7(11)	CP2	1R2	H1-2	122.0
C10	C14	C19	125.6(9)	C4	1R2	1R1	89.7(2)
C13	C14	C19	126.0(10)	C4	1R2	C3	86.1(3)
				C4	1R2	H1-2	94.6(21)
C21	C20	C24	107.2(5)	C3	1R2	H1-2	83.6(20)
C20	C21	C22	107.4(6)				
C21	C22	C23	109.5(5)	C1	C2	C3	119.1(7)
C22	C23	C24	106.1(6)	C2	C3	1R2	121.2(6)
C20	C24	C23	109.5(5)	1R1	C3	1R2	86.9(2)
C21	C20	C25	125.4(7)	1R1	H1-2	1R2	109.3(32)
C24	C20	C25	125.9(6)				
C20	C21	C26	125.5(7)	1R2	C4	C5	123.3(5)
C22	C21	C26	127.1(6)	1R2	C4	C9	122.2(5)
C21	C22	C27	126.3(6)	C5	C4	C9	114.1(7)
C23	C22	C27	123.7(6)	C4	C5	C6	122.3(8)
C22	C23	C28	126.0(6)	C5	C6	C7	122.0(9)
C24	C23	C28	127.1(6)	C6	C7	C8	119.4(9)
C20	C24	C29	125.7(6)	C7	C8	C9	118.6(8)
C23	C24	C29	124.8(6)	C4	C9	C8	123.5(7)

Table III. Selected Bond Distances (Å) for 2

ATOM 1	ATOM 2	DISTANCE
1R1	1R2	2.781(1)
1R1	P	2.201(2)
1R1	C1	2.046(7)
1R1	C11	2.269(6)
1R1	C12	2.241(6)
1R1	C13	2.257(7)
1R1	C14	2.315(7)
1R1	C15	2.335(7)
1R1	CP1	1.940(1)
1R2	C1	2.139(6)
1R2	C2	2.107(7)
1R2	C3	2.112(7)
1R2	C21	2.153(7)
1R2	C22	2.220(9)
1R2	C23	2.296(9)
1R2	C24	2.234(7)
1R2	C25	2.156(7)
1R2	CP2	1.874(1)
1R1'	C1	1.964(10)
1R1'	C3	2.121(11)
1R1'	1R2'	2.729(11)
1R1'	CP1	2.102(8)
1R2'	C1	2.215(10)
1R2'	P'	2.281(7)
1R2'	CP2	2.200(7)
P	C4	1.850(9)
P	C5	1.826(8)
P	C6	1.869(8)
C1	C2	1.421(11)
C2	C3	1.453(11)

Table IV. Selected Bond Angles (deg) for 2

ATOM 1	ATOM 2	ATOM 3	ANGLE
CP1	1R1	1R2	127.84(1)
CP1	1R1	P	127.96(6)
CP1	1R1	C1	140.1(2)
P	1R1	1R2	98.52(5)
P	1R1	C1	86.0(2)
1R2	1R1	C1	49.8(2)
CP2	1R2	1R1	141.13(2)
CP2	1R2	C1	152.0(2)
CP2	1R2	C2	142.6(2)
CP2	1R2	C3	130.5(2)
C1	1R2	C2	39.1(3)
C1	1R2	C3	70.6(3)
C2	1R2	C3	40.3(3)
1R1	1R2	C3	80.9(2)
CP1	1R1'	1R2'	126.0(4)
CP1	1R1'	C1	134.2(5)
CP1	1R1'	C3	146.6(5)
C1	1R1'	C3	73.8(4)
1R2'	1R1'	C3	83.6(4)
CP2	1R2'	1R1'	111.3(3)
CP2	1R2'	P'	142.9(4)
CP2	1R2'	C1	123.8(4)
P'	1R2'	C1	90.6(3)
P'	1R2'	1R1'	102.8(3)
1R1'	1R2'	C1	45.4(3)
1R1	P	C4	116.4(3)
1R1	P	C5	115.7(4)
1R1	P	C6	121.8(3)
C4	P	C5	99.7(5)
C4	P	C6	101.9(5)
C5	P	C6	97.5(5)
1R1	C1	1R2	83.2(2)
1R1'	C1	1R2'	81.3(4)
1R1	C1	C2	121.7(6)
C1	C2	C3	117.5(7)

$\times 10^4$; 341, $\epsilon = 8.8 \times 10^3$; 500, $\epsilon = 4.2 \times 10^3$), probably due to the absence of a metal–metal bond.[17]

This structural assignment was confirmed by a single-crystal X-ray diffraction study. An ORTEP diagram is shown in Figure 4 with selected bond distances and angles given in Tables V and VI, and further data are supplied in the Experimental Section and supplementary material. The most important aspect of this structure is the absence of an iridium–iridium bond (3.833 Å).

The minor complex observed above, **8**, was obtained in higher yield (56%) by heating a benzene solution of either **7** or **2** to 100 °C for 13 days (Scheme V). This complex was identified by standard analytical and spectroscopic information. In the ^{1}H NMR spectrum the two phosphine-bound methyl groups appear at δ 1.60 (d, J_{HP} = 10.5 Hz) and 1.18 ppm (d, J_{HP} = 8.1 Hz) while

(17) A discussion of electronic transitions in transition-metal complexes is given in: DeKock, R. L.; Gray, H. B. *Chemical Structure and Bonding*; Benjamin/Cummings: Menlo Park, CA, 1980.

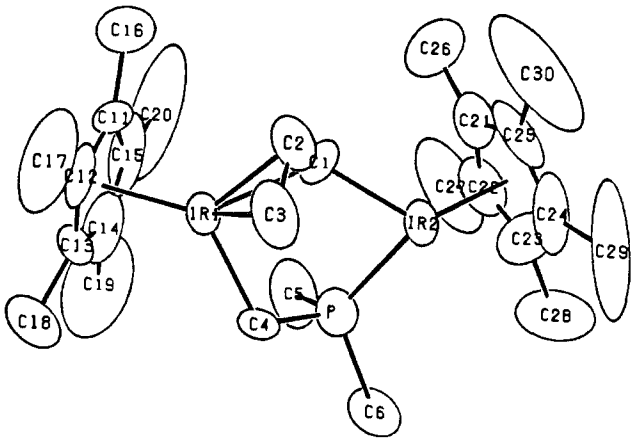

Figure 4. ORTEP diagram of complex of **7**.

Table V. Selected Bond Distances (Å) for 7

ATOM 1	ATOM 2	DISTANCE
1R1	1R2	3.833(1)
1R1	C1	2.195(9)
1R1	C2	2.140(9)
1R1	C3	2.167(10)
1R1	C4	2.130(9)
1R1	C11	2.215(10)
1R1	C12	2.212(8)
1R1	C13	2.193(9)
1R1	C14	2.180(11)
1R1	C15	2.189(10)
1R1	CP1	1.854
1R2	P	2.234(3)
1R2	C1	2.000(8)
1R2	C21	2.278(10)
1R2	C22	2.236(10)
1R2	C23	2.229(12)
1R2	C24	2.192(12)
1R2	C25	2.230(9)
1R2	CP2	1.888
P	C4	1.733(12)
P	C5	1.883(12)
P	C6	1.848(12)
C1	C2	1.428(13)
C2	C3	1.477(15)
C11	C12	1.402(17)
C11	C15	1.435(22)
C12	C13	1.383(15)
C13	C14	1.366(16)
C14	C15	1.355(21)
C11	C16	1.474(18)
C12	C17	1.483(15)
C13	C18	1.535(15)
C14	C19	1.569(18)
C15	C20	1.531(16)
C21	C22	1.404(16)
C21	C25	1.406(16)
C22	C23	1.300(17)
C23	C24	1.426(24)
C24	C25	1.475(21)
C21	C26	1.484(17)
C22	C27	1.595(18)
C23	C28	1.554(19)
C24	C29	1.451(18)
C25	C30	1.524(20)

Scheme V

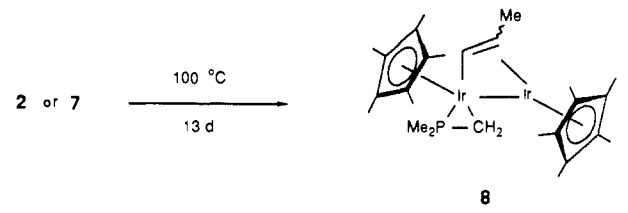

8

Table VI. Selected Bond Angles (deg) for 7

ATOM 1	ATOM 2	ATOM 3	ANGLE
CP1	1R1	C1	134.9
CP1	1R1	C2	128.1
CP1	1R1	C3	134.3
CP1	1R1	C4	126.5
C4	1R1	C1	86.0(3)
C4	1R1	C2	105.4(4)
C4	1R1	C3	86.1(5)
C1	1R1	C2	38.4(4)
C1	1R1	C3	68.8(4)
C2	1R1	C3	40.1(4)
CP2	1R2	P	136.2
CP2	1R2	C1	125.8
P	1R2	C1	82.3(3)
1R1	C1	1R2	126.9(5)
1R2	P	C4	113.7(3)
1R1	C4	P	112.9(5)
C1	C2	C3	116.1(9)
1R2	P	C5	114.9(4)
1R2	P	C6	116.4(4)
C4	P	C5	104.1(5)
C4	P	C6	104.2(6)
C5	P	C6	101.9(7)

Scheme VI

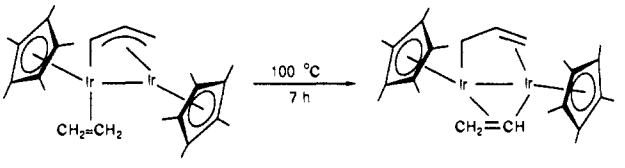

4 9

the methylene protons resonate at δ 0.30 (dd, J_{HP} = 4.5 Hz, $J_{HH(gem)}$ = 10 Hz) and −0.04 ppm (dd, J_{HP} = 8 Hz, $J_{HH(gem)}$ = 10.2 Hz). The ^{1}H NMR spectrum clearly shows the μ-CH proton resonance at δ 6.80 (d, J = 8.9 Hz) while the other CH proton appears at δ 2.0 ppm (m), consistent with coordination of the olefinic carbon to the iridium center. The observed H–H coupling between the two olefinic hydrogens in the η^1,η^2-propenyl ligand (J = 8.9 Hz) does not definitively distinguish between a cis or trans orientation.[18] In the ^{13}C NMR spectrum the phosphine methyl carbons appear at δ 22.37 (q, J_{CP} = 0 Hz, J_{CH} = 127 Hz) and 19.7 ppm (dq, J_{CP} = 50 Hz, J_{CH} = 127 Hz) and the methylene carbon appears at δ −23.5 ppm (dt, J_{CP} = 21 Hz, J_{CH} = 136 Hz). The ^{13}C NMR spectrum also supports the η^1,η^2-propenyl ligand assignment. The methyl carbon appears at δ 24.2 (q, J = 125 Hz) and the olefinic carbons appear at δ 41.7 (d, J = 152.2 Hz) and 107.3 ppm (dd, J_{CP} = 3.1 Hz, J_{CH} = 139.6 Hz). The ^{31}P{^{1}H} NMR (C_6D_6) spectrum shows a single line at δ −89.5 ppm (vs H_3PO_4). The combined spectral data given are consistent with the presence of a η^2-CH_2PMe_2 ligand.[19] Curiously, one of the phosphine methyl groups has a large carbon–phosphorus coupling constant (50 Hz) while the other shows no observable carbon–phosphorus coupling. In support of the above formulation are several reports of other η^2-$CH_2P(Me_2)$ linkages whose ^{31}P{^{1}H} NMR spectra show distinct upfield chemical shifts.[19] Spectral data also support the formation of a η^1,η^2-CH=CHCH$_3$ ligand, which is the overall result of migration of the iridium hydride in **7** into the CH_2 position of the η^1,η^3-allyl ligand.

Heating a C_6H_6 solution of the ethylene complex **4** to 100 °C for 7 h produced an 83% yield of yellow-orange crystals of **9**. Monitoring the reaction by ^{1}H NMR spectroscopy showed no observable intermediates. Spectroscopic and analytical data on

(18) For a description of other μ-alkenyl complexes see: Casey, C. P.; Meszaros, M. W.; Fagan, P. J.; Bly, R. K.; Colborn, R. E. *J. Am. Chem. Soc.* **1986**, *108*, 4053 and references cited therein.

(19) Several η^2-CH_2PMe_2 complexes have been reported. See, for example: ref 15 and (a) Green, M. L. H.; Parkin, G.; Mingqin, C.; Prout, K. *J. Chem. Soc., Dalton* **1986**, 2227. (b) Andersen, R. A.; Mainz, V. V. *Organometallics* **1984**, *3*, 675 and references cited therein.

Scheme VII

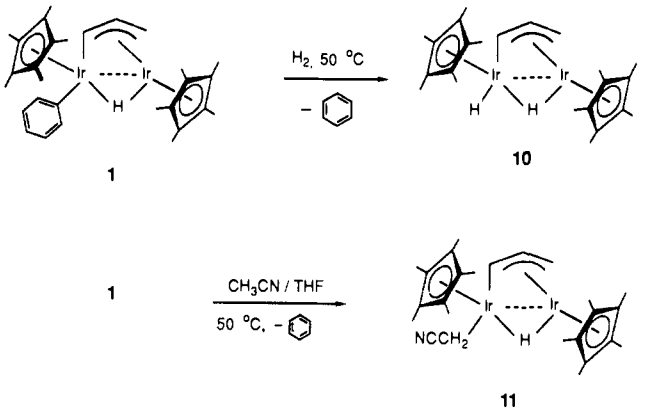

this thermolysis product are most consistent with the formation of a dinuclear allylvinyliridium complex formed by insertion of an iridium center into one of the vinyl C–H bonds, followed by migration of the activated hydrogen atom to the allyl group. Our most reasonable guess for the structure of this insertion product is complex **9** illustrated in Scheme VI. Overall, this transformation involves insertion of iridium into one of the olefinic C–H bonds of the bound ethylene ligand in complex **4** and migration of the hydrogen to the α-carbon of the η^1,η^3-allyl ligand. The bonding mode of the η^2-vinyl group is supported by both the ^{1}H NMR (C_6D_6) and ^{13}C NMR spectra. The CH proton resonates at δ 7.38 (dd, J = 7.1, 9.1 Hz); this downfield shift is consistent with other reported η^2-vinyl complexes.[20] The CH_2 protons appear at δ 3.40 (d, J = 7 Hz) and 2.23 ppm (d, J = 9.2 Hz); the upfield chemical shifts are indicative of bonding of the olefin to an iridium center. The ^{13}C NMR (C_6D_6) spectrum shows the CH carbon at δ 111.2 ppm (d, J = 149 Hz) and the CH_2 carbon at δ 44.2 ppm (dd, J = 159, 146 Hz). The conversion of the η^1,η^3-allyl ligand into the η^1,η^2-allyl group is supported by both the ^{1}H NMR (C_6D_6) and ^{13}C NMR (C_6D_6) data. In the ^{1}H NMR (C_6D_6) spectrum five unique resonances for this group appear at δ 2.85 (m), 2.30 (t, J = 8 Hz), 1.90 (t, J = 6.4 Hz), 1.25 (d, J = 7.8 Hz), and 0.56 ppm (d, J = 10.3 Hz). The ^{13}C NMR (C_6D_6) spectrum shows the η^1,η^2-allyl carbons at δ 34.8 (d, J = 153.5 Hz), 30.9 (t, J = 157 Hz), and −14.1 ppm (t, J = 134 Hz). The upfield carbon resonance at δ −14.1 ppm clearly shows the transformation of the bridging α-carbon in **4** (δ 119.9; d, J = 152.7 Hz) to the singly bound CH_2 in **9**. Although this structure appears to rationalize our spectral data most easily, they do not allow us to rigorously determine the geometry of this product, nor to clearly establish which of the two iridium centers is σ-bound to the vinyl group.

Reactions of 1 with Dihydrogen and Acetonitrile: Formation of $(\eta^5$-$C_5Me_5)(R)Ir(\eta^1,\eta^3$-$C_3H_4)(\mu$-$H)Ir(\eta^5$-$C_5Me_5)$ [R = H (10) and CH_2CN (11)]. Thermolysis of a hexane solution of **1** under ca. 1 atm of H_2 gave a red-orange product which, on the basis of spectroscopic and analytical data, was formulated as dinuclear dihydride **10** (Scheme VII). The hydride ligands are clearly distinct and nonfluxional at room temperature by ^{1}H NMR (C_6D_6 and C_6D_{12}) analysis;[21] δ −18.3 (s) and −18.5 ppm (s) in C_6D_6 and δ −18.5 (s) and −19.25 ppm (s) in C_6D_{12}. A terminal Ir–H stretch in the solid-state IR (KBr) appears at 2085 cm^{-1}. Although no direct spectroscopic evidence establishes the presence of bridging rather than terminal hydrides, we feel that our assignment is correct based on the analogy to **1** and the similar product formed from the thermolysis of **1** with acetonitrile (vide infra).

Thermolysis of **1** in a 10/1 mixture of THF/acetonitrile gave acetonitrile C–H insertion product **11** in 67% yield (Scheme VII). The structure of this complex was assigned on the basis of spectroscopic information. In the ^{1}H NMR (C_6D_6) spectrum the acetonitrile methylene hydrogens appear at δ 1.50 (d, $J_{HH(gem)}$ = 14.2 Hz) and 1.11 ppm (d, $J_{HH(gem)}$ = 14.2 Hz) while the acetonitrile carbon atoms appear at δ 130.8 (t, $^2J_{CH}$ = 7.3 Hz) and −29.7 ppm (t, J = 136.8 Hz) in the ^{13}C NMR spectrum. The solid-state IR (KBr) shows a sharp CN stretch at 2195 cm^{-1}. The presence of diastereotopic methylene protons and the upfield carbon resonance in the ^{13}C NMR spectrum support the presence of a CH_2CN ligand. The upfield resonance at δ −21.0 ppm (s) in the ^{1}H NMR (C_6D_6) spectrum and the absence of an Ir–H stretch in the infrared spectrum suggest the presence of a μ-hydride linkage.

Table VII. Rate Constants for Thermal Conversion of **1** to **2**[a]

[1] x 10^5	[PMe_3] x 10^3	k_{obs} x 10^3 (s^{-1})
1.6	340	4.0
6.5	340	4.3
6.5	68	4.21
6.5	16	4.5
6.5	3.2	4.7

[a] In hexane at 50 °C. Standard deviation in each run was <1%; reproducibility is ±3%.

Scheme VIII

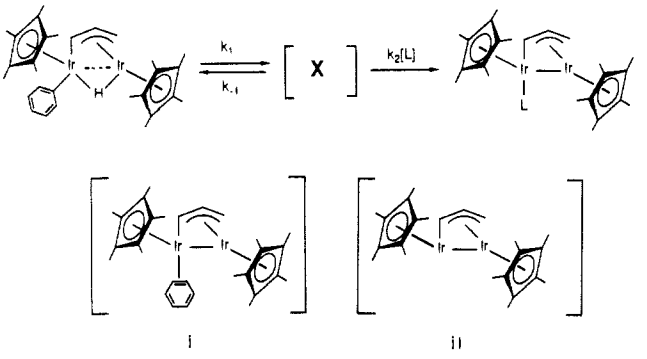

Mechanistic Study of the Reductive Elimination of Benzene from 1. Kinetic Studies. The formal reduction of each iridium center in **1** upon addition of dative two-electron donor ligands is a rare example of a dinuclear reductive elimination process.[22] For this reason we explored the mechanism of this reaction.

The order of each component in the rate of the reductive elimination reaction between **1** and PMe_3 was established by obtaining kinetic data by both UV–visible spectroscopy and ^{1}H NMR analysis. In all cases the rate of reaction was determined under pseudo-first-order conditions and followed through at least 3 half-lives. From these results the reaction shown in Scheme II clearly shows a first-order dependence on complex **1** and zero-order dependence on PMe_3 at all concentrations of PMe_3 used (the measured rate constants are given in Table VII). This result precludes any involvement of free PMe_3 in the rate-determining step of the reaction under these conditions (however, see below). Using $P(OCH_3)_3$ in place of PMe_3 did not affect the first-order decay rate of **1** (k_{obs} = 1.65 × 10^{-4} at 45 °C in C_6D_{12}). These results imply the first-order transformation of **1** into an intermediate X, which is then rapidly trapped by L to give the final products (Scheme VIII).

To test the possibility that the formation of the intermediate from **1** is reversible, and to determine whether free benzene is formed in the first or second step, rate studies were conducted with varying [C_6H_6]/[PMe_3] ratios. The results of this study are given in Table VIII. A plot of $1/k_{obs}$ vs. [C_6H_6]/[PMe_3] is given in Figure 5. The linearity of this plot is consistent with a mechanism in which the starting material undergoes equilibration

(20) In $(\mu$-H)$(\mu$-CH=$CH_2)Re_2(CO)_8$: δ 7.18 ppm for vinylic CH, ref 2b.

(21) In this complex it is not certain which resonance in the ^{1}H NMR spectrum is the terminal hydride and which is the bridging hydride. On the basis of analogy to the other bridging hydride species in this paper, the upfield resonance is tentatively assigned as the bridging hydride.

(22) The presence of a bridging metal hydride raises the question as to whether this is truly a "dinuclear" reductive elimination reaction. Complex **1** may be either an $Ir^{II.5}$–Ir^{III} or Ir^{IV}–Ir^{II} system, or some hybrid of the two. The final product **2** is best described as an Ir^{II}–Ir^{II} system.

Table VIII. Benzene Inhibition Studies: Rate of Reaction between 1 and PMe_3 with Added Benzene[a]

$[C_6H_6]$	$[PMe_3] \times 10^3$	$[C_6H_6]/[PMe_3] \times 10^{-2}$	$k_{obs} \times 10^5$	$1/k_{obs} \times 10^{-3}$
11.2	32.2	3.5	18.1	5.53
11.2	10.7	10.5	12.8	7.81
11.2	4.3	26.3	8.4	11.9
11.2	2.1	52.5	4.4	22.7

[a] All runs at 50 °C. Standard deviation <1%; reproducibility (checked in run No. 1) is ±2%.

Table IX. Temperature Dependence of Rate of Conversion of 1 to 2[a]

Temperature °C	$k_{obs} \times 10^5$ (s^{-1})	$1/T\ °K \times 10^{-3}$
35	7.9	3.247
40	14	3.195
45	24	3.145
50	43	3.096
55	78	3.049
60	140	3.003
65	200	2.959

[a] In hexane [1] = 6.5×10^{-5}, $[PMe_3] = 3.4 \times 10^{-1}$. Standard deviation in each run: <1%; reproducilibity estimated as ±2%.

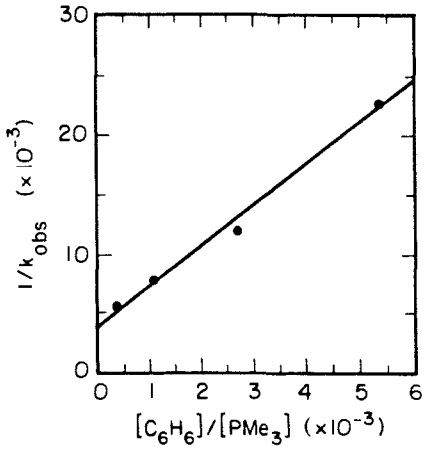

Figure 5. Plot of $1/k_{obs}$ vs $[C_6H_6][PMe_3]$ for the reaction between 1 and PMe_3.

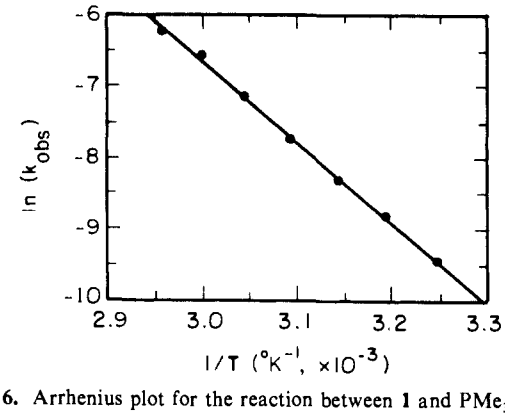

Figure 6. Arrhenius plot for the reaction between 1 and PMe_3.

with a transient intermediate X and free benzene (eq 1), followed by reaction of X with PMe_3 (eq 2). This gives the rate law shown in eq 3 and the reciprocal relationship given in eq 4.

$$1 \underset{k_{-1}}{\overset{k_1}{\rightleftharpoons}} X + C_6H_6 \quad (1)$$

$$X + PMe_3 \xrightarrow{k_2} \text{products} \quad (2)$$

$$\text{rate} = -\frac{d[1]}{dt} = \frac{k_1k_2[PMe_3]}{k_{-1}[C_6H_6] + k_2[PMe_3]}[1] = k_{obs}[1] \quad (3)$$

$$1/k_{obs} = \frac{k_{-1}[C_6H_6]}{k_1k_2[PMe_3]} + \frac{1}{k_1} \quad (4)$$

Scheme IX

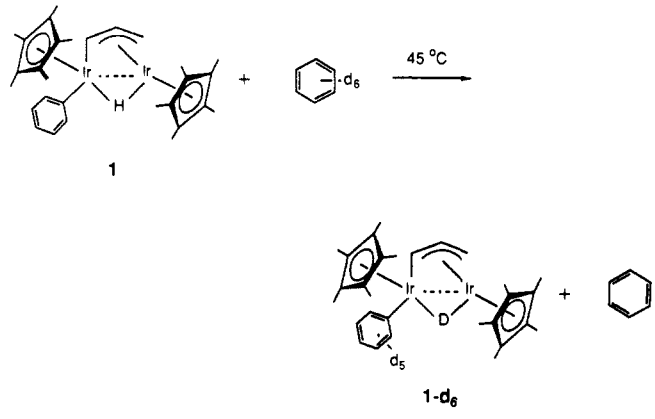

At high benzene and PMe_3 concentrations, pseudo-first-order kinetics are observed, allowing measurement of the $[C_6H_6]/[PMe_3]$ dependent rate constant, k_{obs}. From the slope of the plot in Figure 5 $k_2/k_{-1} = 1120$, and from the intercept $k_1 = 2.6 \times 10^{-4}$ s^{-1}. The reversibility of the reductive elimination step k_1 was also established by the observation that thermolysis of 1 in C_6D_6 at 45 °C gave clean isotopic exchange; the observed rate constant for this process is $k_{obs} = 1.5 \times 10^{-4}$ s^{-1} (Scheme IX).

To gain more information about the loss of benzene from 1 we measured the rates of the reaction at various temperatures; the results are given in Table IX. An Arrhenius plot is shown in Figure 6 from which we calculate $\Delta S^{\ddagger} = -6$ eu and $\Delta H^{\ddagger} = 22.1$ kcal mol^{-1}.

Isotope Effects. To explore the nature of the intermediate X the isotope effect in the reductive elimination was determined. For these studies 1 isotopically labeled in the phenyl group and the bridging hydride position was required.[23] We employed 1-d_{10}, prepared as described in the Experimental Section; the identity of this deuteriated product was established by standard spectroscopic means. The rate of reaction between 1-d_{10} and PMe_3 was carried out at 50 °C; $k_D = 5.95 \times 10^{-4}$. From this rate and that obtained with 1, $k_H/k_D = 0.72 \pm 0.03$ (error determined by standard error analysis of standard deviations in each run).

To gain more information on the intermediate's ability to insert into the benzene C-H bond, both the intra- and intermolecular isotope effects for this process were obtained. The proposed intermediate X was generated at ca. 6 °C by irradiation of the CO complex 3. For the intermolecular case the irradiation was conducted in a 1:1 ratio of C_6H_6/C_6D_6, and by measuring the integrated ratio of proton resonances in the aromatic group vs the proton resonances in the η^1,η^3-allyl group k_H/k_D(inter) was determined to be 1.54 ± 0.04 (based on 3 runs): see Scheme X. Irradiation of 3 in 1,3,5-$C_6D_3H_3$ gave k_H/k_D(intra) = 1.63 ± 0.15 (error based on inherent uncertainty in integration of proton resonances in the aromatic region of the product; see Scheme X).

In a crossover experiment designed to investigate the intramolecularity of the reductive elimination, a 1:1 mixture of 1 and 1-d_{10} was allowed to react with ethylene at 50 °C for 24 h. The volatile materials were collected; only C_6D_6 and C_6H_6 were observed by GC mass spectrometry (Scheme XI). The absence of C_6D_5H and C_6H_5D shows the intramolecular nature of the process.

(23) Deuteriation of the π-allyl ligand occurs readily under the exchange conditions used: see ref 5b.

Scheme X

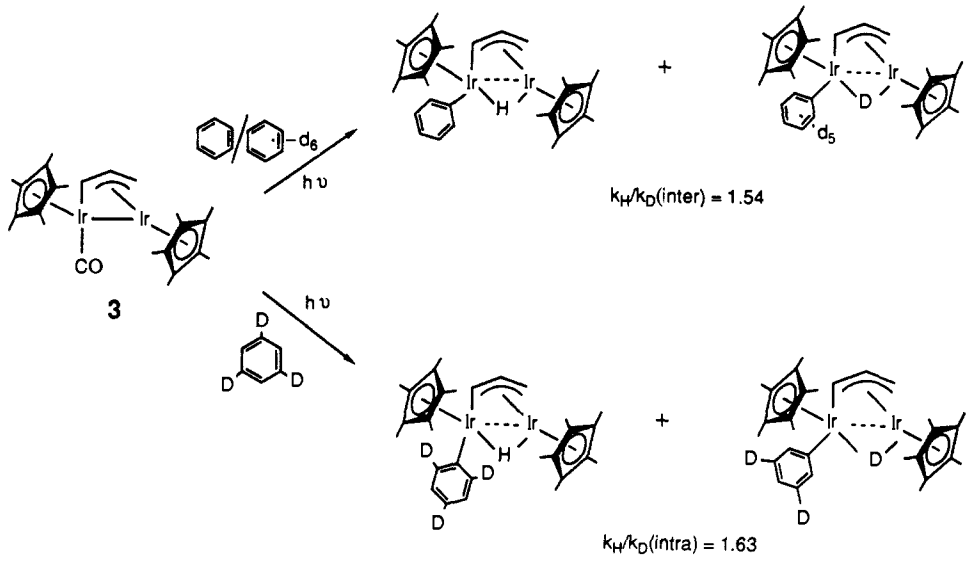

Scheme XI

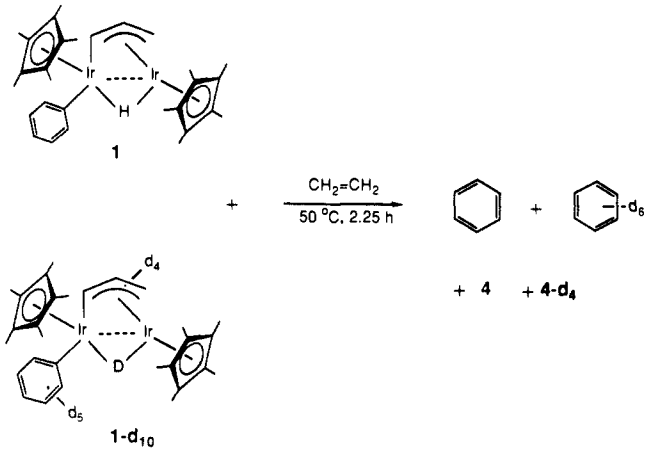

Mechanistic Study of Intramolecular C–H Insertion in 2. The oxidative addition of the C–H bond in the PMe_3 ligand in **2** across the metal–metal bond leading to **7** (Scheme IV) was unexpected and therefore also warranted mechanistic investigation. The rate of disappearance of **2** was cleanly first order through at least 3 half-lives and was unaffected by the addition of free PMe_3 ($k_{obs} = 1.33 \times 10^{-4}$ s^{-1}; with 0.4 M PMe_3, $k_{obs} = 1.22 \times 10^{-4}$ s^{-1}). This result implies that the bound PMe_3 ligand does not dissociate reversibly during the course of the reaction. To further support this conclusion we carried out the thermolysis reaction in the presence of $P(CD_3)_3$. No incorporation of $P(CD_3)_3$ was observed in either the starting material or the final product.

Replacement of PMe_3 in **2** with $P(CD_3)_3$ was accomplished by addition of $P(CD_3)_3$ to a hexane solution of **1** and warming the solution to 45 °C for 16 h (Scheme XII). The deuteriated product was characterized by ^{1}H NMR, ^{13}C{^{1}H} NMR, ^{31}P{^{1}H} NMR, and ^{2}H{^{1}H} NMR spectrometry, mass spectrometry, and UV–visible spectroscopy (see Experimental Section). Heating a C_6D_6 solution of **2**-d_9 to 80 °C (20 °C below the temperature required for the thermal C–H bond cleavage reaction with **2**) produced scrambling of deuterium into the α-allylic position of **2** as determined by ^{1}H NMR and ^{2}H{^{1}H} NMR spectrometry (Scheme XII). Raising the temperature to 100 °C gave **7**-d_9, deuteriated as shown in the scheme.

The unexpected scrambling reaction with **2**-d_9 at 80 °C led us to investigate the thermolysis of complex **4** prepared with tetradeuterioethylene. Heating a solution of **4**-d_4 in C_6D_6 to 80 °C gave no apparent reaction. Continued heating to 100 °C gave only the C–D cleavage reaction product (as with **4**, shown in Scheme VI) with no observable scrambling of deuterium in the starting material.

Discussion

Mechanism of the Synthesis and Reactions of Dinuclear Hydridophenyliridium Complex 1. The majority of the new complexes reported in this paper, along with reasonable mechanistic pathways for interconversion of these materials, are summarized in Scheme

Scheme XII

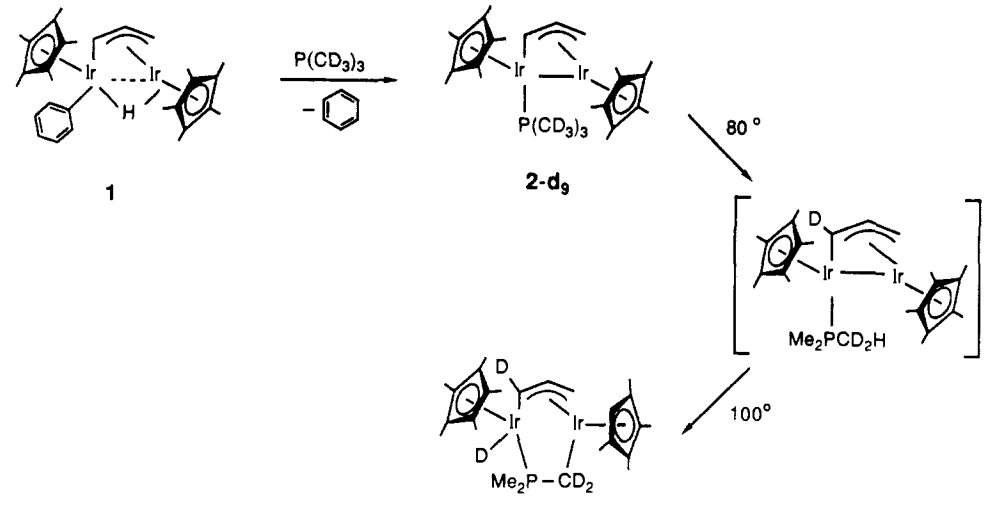

Scheme XIII

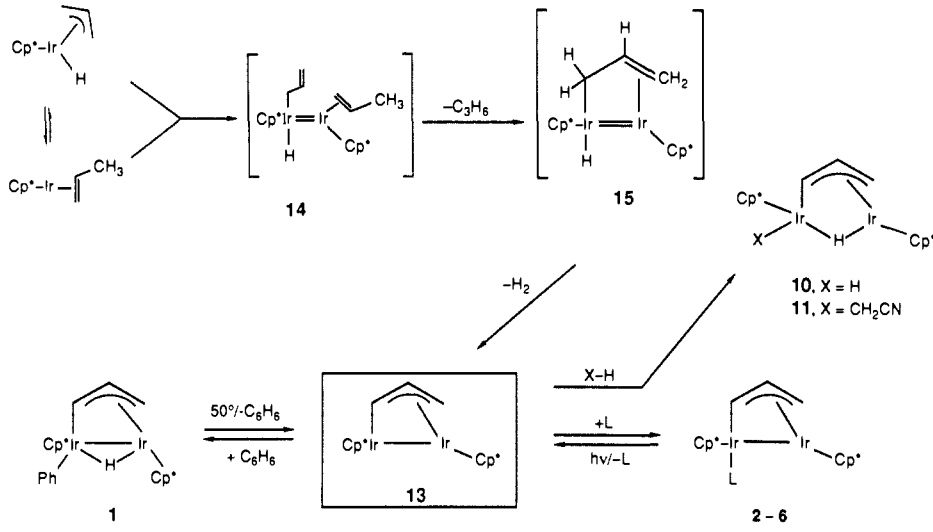

Scheme XIV

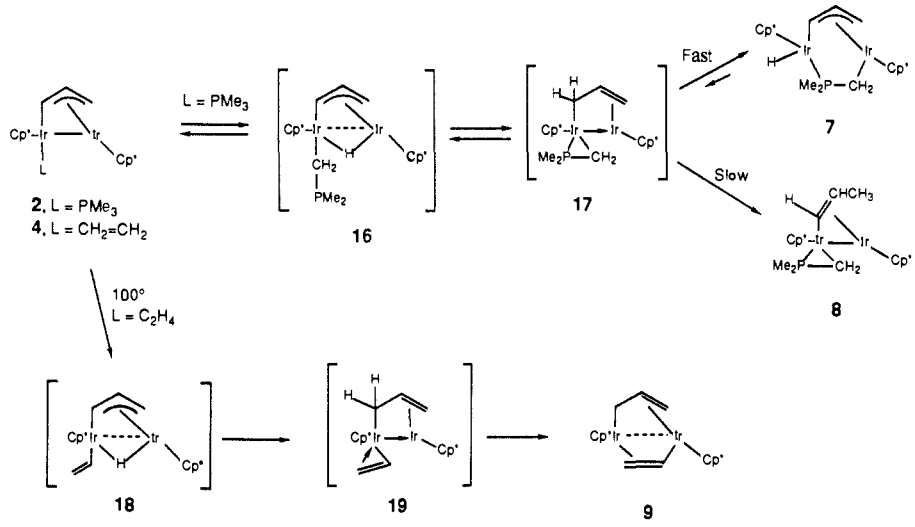

XIII and XIV. A significant fraction of this chemistry may be understood in terms of the properties of the coordinatively unsaturated dinuclear intermediate **13** or a solvated analogue of this material.

We observed earlier[5b] that thermolysis of dilute solutions of the π-allyl hydride $(\eta^5\text{-}C_5Me_5)(\eta^3\text{-}C_3H_5)(H)Ir$ in benzene led to the mononuclear arene C-H activation product $(\eta^5\text{-}C_5Me_5)(PMe_3)(Ph)(n\text{-}C_3H_6)Ir$. A case was made that this reaction proceeded by initial reductive elimination, giving the intermediate propene π-complex $(\eta^5\text{-}C_5Me_5)(H_2C{=}CHCH_3)Ir$. Because this material is a coordinatively unsaturated Ir(I) complex, it is capable of inserting into the C-H bonds of benzene. Our observation of this process led to the study reported in the earlier account.[5b]

At higher concentrations, a greater probability exists that the unsaturated propene complex can react competitively with a second molecule of starting allyl hydride. The ultimate product of this reaction is the dinuclear benzene C-H activation product **1**, the subject of this paper. We have not investigated the mechanism of formation of **1**. However, a reasonable hypothesis is outlined in Scheme XIII. Interaction of the π-propene complex with the allyl hydride (perhaps as its η^1 isomer) could lead to transient dinuclear species **14**. Intramolecular displacement of propene gives **15**, followed by loss of H_2 (perhaps via an α-elimination step involving the allyl ligand) to generate intermediate **13**. Reaction of this species with benzene then leads to **1**. Overall, therefore, conversion of the starting allyl hydride to **1** involves intramolecular activation of a C-H bond in the allyl ligand and intermolecular insertion of the dimetal center into a C-H bond of benzene.

The role played by coordinatively unsaturated dinuclear species **13** in this chemistry is reinforced by mechanistic evidence implicating its intervention in further transformations of **1**. Thermal reactions of **1** with various substrates occur under mild conditions (50 °C in benzene). The existence of an intermediate in this process is demonstrated by a first-order rate law and the absence of a rate dependence on the concentration of entering ligand. The reductive elimination of benzene was shown to be intramolecular, ruling out a bimolecular mechanism involving two molecules of **1**.

That the intermediate is **13** (or a solvated version of this species) is suggested by its trapping with dative ligands L to give adducts **2-6**, and by its reaction with isotopically labeled benzene (as postulated in the formation of **1**), generating **1**-d_6. The relative rate with which PMe_3 and benzene trap the intermediate (k_2/k_{-1}; cf. Figure 5 and eq 1 and 2) is 1120, favoring the phosphine. This result is not surprising in view of the relative nucleophilicities of the two entering ligands.

To further explore the benzene C-H (C-D) insertion step, the method of comparative intermolecular vs intramolecular isotope effects was used.[24] The values obtained in our study (both close to 1.6) show no significant difference between the two types of effects. Both this result and the magnitude of the effect contrast with the observations reported by Jones and Feher in their studies involving the C-H activation of arenes with $(\eta^5\text{-}C_5Me_5)Rh$-

(24) (a) Dolbier, W. R.; Dai, S.-H. *J. Am. Chem. Soc.* **1972**, *94*, 3946. (b) Dolbier, W. R.; Dai, S.-H. *Ibid.* **1968**, *90*, 5028.

(PMe_3).[25] These workers found a significant difference between the intra- (1.4) and intermolecular (1.05) effects in their system. They accounted for this by postulating intervention of a second intermediate, an η^2-arene complex, in the C–H insertion step. The magnitude of our isotope effect is most consistent with its operating in the insertion step. However, the identity of our inter- and intramolecular effects does not allow us to definitively determine whether a second intermediate (ie., an η^2-arene complex) intervenes in this reaction. While it is possible that such a species is involved, the most economical interpretation of our results postulates the intermediacy of **13** rather than the analogous complex having benzene π-coordinated to one of the iridium centers. Direct insertion into the C–H bond of ethylene without prior π-coordination of the olefin has been observed earlier.[26]

Additional evidence for the intermediacy and properties of **13** was provided by its oxidative addition reactions with molecules other than benzene, and its generation by irradiative loss of ligand from trapping products **3** and **4**. Thus, reaction of **13** with H_2 and acetonitrile gave oxidative addition products **10** and **11**, respectively (Scheme XIII). Attempts to insert **13** into the C–H bonds of saturated hydrocarbons have thus far failed in this system. Even if an alkyl analogue of **1** were formed, its isolation under ambient conditions might be problematical in light of the mild conditions required for reductive elimination of benzene in **1**. Construction of similar complexes with more basic ligands may stabilize such alkyl hydrides toward reductive elimination, as is observed in mononuclear systems such as $(\eta^5\text{-}C_5Me_5)(L)Ir(R)H$.[27]

Because of the intervention of other processes (see below), it did not prove possible to regenerate **13** thermally from ligand-trapped products **2–6**. However, irradiation of CO and ethylene complexes **3** and **4** in benzene did give rise to **1**, again presumably by ligand loss to give the dinuclear coordinatively saturated intermediate.

Intramolecular C–H Activation Reactions. Intramolecular C–H activation in this system is not limited to the allyl C–H α-elimination reaction that presumably occurs during the conversion of **15** to **13** (cf. Scheme XIII). This type of transformation was observed in the thermal reactions of both PMe_3 complex **2** and ethylene complex **4**, leading to rearranged final products **7** and **9**.

Kinetic and labeling experiments provided some information about the mechanism of these transformations. The thermolysis of phosphine complex **2** follows a simple first-order rate law. The intramolecularity of the cyclometalation was confirmed by the lack of inhibition in the rate of reaction upon addition of free PMe_3 and by the absence of ligand exchange in the presence of $P(CD_3)_3$. This indicates that PMe_3 does not dissociate in the thermolysis reaction and intermediate **13** is not involved in the process. Interestingly, heating deuteriated phosphine complex **2**-d_9 at temperatures below that required to convert **2** to **7** showed hydrogen–deuterium scrambling into the α-position of the allyl ligand in the starting material. This rearrangement must occur through an intermediate with a structure different from that of stable complex **7**. A possible mechanism for this process, which also accounts for the formation of **7** and **8**, is outlined in Scheme XIV. We suggest that the reaction is initiated by C–H activation of the coordinated phosphine ligand, leading to intermediate **16**, which is analogous to the intermolecular C–H activation products **1**, **10**, and **11**. Coordination of the phosphorus atom then drives migration of the iridium-bound hydrogen to the α-position of the allyl ligand, giving **17**.

We suggest that intermediate **17** serves as a branch point for the three processes observed in this system. Return to **16** and **2** (the most rapid process) leads to deuterium scrambled starting material. The next most favorable process involves return of the allyl-bound hydrogen to iridium, along with migration of the cyclometalated CH_2 group to the second metal center, leading to **7**. Finally, we propose that pyrolysis of **7** reversibly regenerates small concentrations of **17**. This allows access to the slowest reaction channel for this intermediate, which involves 1,3-hydrogen migration in the allyl ligand, leading to dinuclear vinyl complex **8**.

Deuteriated ethylene complex **4**-d_4 gives a different type of final product on thermolysis, but its structure provides support for intermediates suggested in the reactions of phosphine complex **2**. As in the case of **2**, we propose that the reaction is initiated by oxidative addition of the vinyl C–H bond to the iridium center to which the alkene is coordinated, leading to intermediate **18**. In analogy to the **16** → **17** reaction, we then propose π-electron-assisted migration of hydrogen to the allyl group, leading to **19**. Shift of the vinyl group to the adjacent iridium then gives the final product **9**. Further experiments will be required to understand why the mobile hydrogen atom prefers to reside on the allyl group in **9** but moves back to the iridium center in phosphine analogue **7**.

Conclusions

The dinuclear iridium complexes discussed in this paper undergo intermolecular insertion into activated carbon–hydrogen bonds, such as those in benzene and acetonitrile. Because reductive elimination of arene from the benzene C–H activation product occurs more easily than it does in $(\eta^5\text{-}C_5Me_5)(PMe_3)Ir(Ph)(H)$, it may be that alkane C–H activation products can be formed transiently but are not thermodynamically stable in this system. Intramolecular C–H activation of coordinated PMe_3 and ethylene is also observed, although the materials isolated in these reactions result from rearrangement of the initially formed insertion products. This work demonstrates that the attachment of a second metal to a C–H activating iridium center modifies, but does not destroy, its propensity for insertion into C–H bonds. It is our hope that other systems, incorporating metals or ligands with different steric and electronic properties, will allow us to extend dinuclear C–H activation to simple alkanes.

Experimental Section

General. All manipulations were conducted under nitrogen or argon by standard drybox, Schlenk, or vacuum line techniques, unless otherwise noted. Experiments conducted in the drybox used a prescrubbed recirculating atmosphere of nitrogen in a Vacuum Atmospheres HE-533 Dri-Lab with attached MO-40-1 Dri-Train and equipped with a −40 °C freezer. Infrared (IR) spectra were recorded on either a Perkin-Elmer Model 283 grating spectrometer or a Perkin-Elmer Model 1550 Fourier transform spectrometer equipped with a Model 7500 Professional Computer.

^1H NMR spectra were obtained at ambient temperature unless otherwise noted on either a Bruker AM-500 or a 300 MHz instrument assembled by Rudi Nunlist at the University of California, Berkeley, NMR facility. Chemical shifts are reported in units of parts per million (ppm) (δ) downfield from tetramethylsilane (Me_4Si). ^1H NMR shifts are recorded relative to residual protiated solvent: benzene-d_5, 7.15; cyclohexane-d_{11}, 1.38; tetrahydrofuran-d_7, 3.53 and 1.78; $CHDCl_2$, 5.32. ^{13}C NMR spectra were recorded at 75.5 or 125.7 MHz, and chemical shifts are given relative to the solvent resonance: benzene-d_6, 128.0; THF-d_8, 67.5. $^{31}P\{^1H\}$ NMR spectra were recorded at 121.5 MHz, and chemical shifts are given relative to external 85% H_3PO_4. All coupling constants are reported in hertz, multiplicities assigned as follows: s, singlet; d, doublet; t, triplet; q, quartet; m, multiplet.

Ultraviolet–visible spectra were recorded on a Hewlett Packard Model 8450 UV/VIS spectrophotometer. Samples were prepared in the drybox and spectra recorded with use of a cuvette fused to a Kontes vacuum stopcock.

Mass spectra were obtained at the UCB mass spectrometry facility on AEI MS-12 and Finnigan 4000 mass spectrometers. Elemental analyses were performed by the UCB microanalytical laboratory. Melting points were recorded in sealed capillary tubes under nitrogen on a Thomas-Hoover capillary melting point apparatus and are uncorrected. Kinetic experiments were run in flame-sealed NMR tubes and were heated in either a Neslab Model RTE-8DD circulating water bath or a Neslab Model EX-250 HT high-temperature oil bath.

Sealed NMR tubes were prepared by fusing Wilmad 505-PS 7 in. NMR tubes to glass joints that were subsequently attached to Kont :s

(25) (a) Jones, W. D.; Feher, F. J. *J. Am. Chem. Soc.* **1986**, *108*, 4814. Evidence for η^2-arene complexes has also been obtained recently in platinum C–H activation reactions: (b) Hackett, M.; Ibers, J. A.; Whitesides, G. M. *J. Am. Chem. Soc.* **1988**, *110*, 1436.

(26) See, for example: (a) Berry, D. H.; Eisenberg, R. *J. Am. Chem. Soc.* **1985**, *107*, 7181. (b) Stoutland, P. O.; Bergman, R. G. *Ibid.* **1985**, *107*, 4581.

(27) For $(\eta^5\text{-}C_5Me_5)Ir(PMe_3)$ chemistry see ref 1g. For $(\eta^5\text{-}C_5Me_5)Ir(CO)$ chemistry see ref 14a,b.

vacuum stopcocks. All samples were degassed by 3 freeze-pump-thaw cycles on a vacuum line. "Glass bombs" refer to cylindrical, medium-walled Pyrex vessels joined to Kontes K-826510 high-vacuum Teflon stopcocks. Gas-phase mass measurements were performed by measuring the pressure in calibrated known-volume bulbs with a MKS Baratron connected to a high-vacuum line.

Unless otherwise stated, all solvents and reagents were purchased from commercial suppliers and used without further purification. Pentane and hexane were distilled from $LiAlH_4$ and CH_3CN from CaH_2 under nitrogen. Benzene, toluene, diethyl ether, and tetrahydrofuran were distilled from sodium benzophenone ketyl under nitrogen. Benzene-d_6 and THF-d_8 were dried over benzophenone ketyl, cyclohexane-d_{12} was dried over sodium, acetone-d_6 was dried over Linde 4A molecular sieves, and CD_2Cl_2 was dried over CaH_2; all deuteriated solvents were vacuum transferred prior to use. 1,3,5-$C_6D_3H_3$ was purchased from MSD isotopes and used as received. Trimethylphosphine (PMe_3) was purchased from Strem, dried over 1:5 Na:K alloy, and used exclusively by vacuum transfer. Acetonitrile was dried over CaH_2 and distilled under nitrogen prior to use. Trimethyl phosphite was dried over sodium and vacuum transferred prior to use. $P(CD_3)_3$ was prepared as described in the literature.[15] Ethylene-d_4 (98% D) was purchased from Stohler Isotope Chemicals and used as received.

(η^5-C_5Me_5)(C_6H_5)Ir(μ-H)(η^1,η^3-C_3H_4)Ir(η^5-C_5Me_5) (1). A glass bomb was charged with 465 mg (1.26 mmol) of (η^5-C_5Me_5)Ir(η^3-C_3H_5)H[6] and 2 mL of C_6H_6 in the drybox. The bomb was sealed and the reaction vessel was removed to the vacuum line. The resulting clear solution was degassed and then heated to 45 °C for 6 days. The volatile materials were removed leaving a brown-orange residue. The residue was dissolved in hexane and the solution cooled to −40 °C in the drybox freezer giving 275 mg (0.36 mmol, 57%) of red-orange, analytically pure crystals of **1**. IR (KBr) 3043 (m), 2968 (s), 2905 (s), 1567 (s), 1466 (s), 1380 (s), 1030 (s), 735 (s); ^{1}H NMR (C_6D_6) δ 7.78 (d, J = 5.4 Hz, 1 H), 7.67 (d, J = 7.1 Hz, 2 H), 7.13 (t, J = 7.4 Hz, 2 H), 6.98 (t, J = 7.2 Hz, 1 H), 5.25 (m, 1 H), 2.13 (d, J = 5.6 Hz, 1 H), 1.79 (s, 15 H), 1.54 (s, 15 H)8 1.27 (br d, J = 7.6 Hz, 1 H), −20.48 (s, 1 H); ^{13}C NMR (C_6D_6) δ 143.8 (s), 142.8 (d, J = 153.5 Hz), 126.8 (d, J = 153 Hz), 120.7 (d, J = 157 Hz), 105.8 (d, J = 154.3 Hz)8 90.9 (s), 90.2 (s), 84.2 (d, J = 156.1 Hz), 31.0 (br t, J = 155 Hz), 10.34 (q, J = 126.7 Hz), 9.8 (q, J = 127.3 Hz); MS, m/e 772, 694, 78 (M^+, $M^+ - C_6H_6$, base); UV (hexane) λ_{max} 340 ($\epsilon = 3.6 \times 10^3$), 460 ($\epsilon$ = 650). Anal. Calcd for $C_{29}H_{40}Ir_2$: C, 45.08; H, 5.18. Found: C, 45.14; H, 5.23.

Single-Crystal X-ray Diffraction Study of 1. Red-orange, block-like crystals of **1** were obtained by slow crystallization from toluene/hexane. Fragments cleaved from some of these crystals were mounted on glass fibers with polycyanoacrylate cement and then coated with quick-setting epoxy. Precession photographs indicated triclinic Laue symmetry and yielded preliminary cell dimensions.

The crystal used for data collection was then transferred to our Enraf-Nonius CAD-4 diffractometer and centered in the beam.[28] It was cooled to −45 ± 4 °C by a nitrogen flow apparatus that had been previously calibrated against a thermocouple placed in the sample position. Attempts to cool below this temperature led to fracture of the sample. Automatic peak search and indexing procedures yielded a triclinic reduced primitive cell with twice the volume of that determined from the photos. Inspection of the Niggli values revealed no conventional cells of higher symmetry.[28b] The final cell parameters and specific data collection parameters are given in Table X.

The 6811 raw intensity data were converted to structure factor amplitudes and their esds by correction for scan speed, background, and Lorentz and polarization effects. No correction for crystal decomposition was necessary. Inspection of the azimuthal scan data showed a variation I_{min}/I_{max} = 0.52 for the average curve. Since the crystal had poorly defined faces and was coated in epoxy, an empirical correction for absorption, based on the azimuthal scan data, was applied to the intensities. A spherical absorption correction based on a sphere of the same volume as the crystal was also applied. The range of transmission for the empirical correction was 0.52 to 0.97, and that for the spherical absorption correction was 0.114 to 0.130 (μR = 1.57).

The structure was solved by Patterson methods and refined via standard least-squares and Fourier techniques. The assumption that the space group was centric ($P\bar{1}$) was confirmed by the successful solution and refinement of the structure. In a difference Fourier map calculated following refinement of all non-hydrogen atoms with anisotropic thermal parameters, peaks corresponding to the expected positions of most of the hydrogen atoms were found. The hydride hydrogens and those on the allyl moiety were included in subsequent refinements with isotropic thermal parameters. "Uninteresting" hydrogens were included in the structure factor calculations in their expected positions based on idealized bonding geometry but were not refined in least squares. All predicted hydrogens were assigned isotropic thermal parameters 1–2 A^2 larger than the equivalent B_{iso} of the atom to which they were bonded.

The final residuals for 600 variables refined against the 5177 data for which $F^2 > 3\sigma(F^2)$ were R = 2.48%, wR = 3.37%, and GOF = 1.589. The R value for all 6811 data was 4.32%.

The quantity minimized by the least-squares program was $\sum w(|F_o| - |F_c|)^2$, where w is the weight of a given observation. The p factor used to reduce the weight on intense reflections was set to 0.03 throughout the refinement. The analytical forms of the scattering factor tables for the neutral atoms were used and all non-hydrogen scattering factors were corrected for both the real and imaginary components of anomalous dispersion.[28c]

Inspection of the residuals ordered in ranges of sin (θ)/λ, $|F_o|$, and parity and value of the individual indexes showed no unusual features or trends. There was no evidence of secondary extinction in the low-angle, high-intensity data. The largest peak in the final difference Fourier map had an electron density of 1.3 $e^-/Å^3$. All peaks with densities of greater than 0.5 $e^-/Å^3$ were located near the Ir atoms. Selected bond distances and angles are given in Tables I and II. The positional and thermal parameters of the atoms and a listing of F_o and F_c are included with the supplementary material for the preliminary communication.[5c]

The structure consists of molecules of **1** packed in a pseudo-A-centered array in the unit cell. The packing does not show any abnormally short intermolecular distances.

An ORTEP drawing of one of the molecules in the asymmetric unit is shown in Figure 1. The molecule has a singly bonded Ir–Ir fragment that is bridged by a hydride atom and by the allyl moiety. The allyl group is π-bonded to Ir1 and σ-bonded through C3 to the other Ir atom in the molecule. The least-squares planes listing shows that all corresponding planes in the two molecules are parallel to within 3° of each other with the exception of the Ir–Ir–C (phenyl) planes, which are inclined 5.3° to each other. This difference in orientation and the difference in the torsion angles around the Ir1–Cp centroid vector constitute the major difference between the two independent molecules.

(η^5-C_5Me_5)(PMe_3)Ir(η^1,η^3-C_3H_4)Ir(η^5-C_5Me_5) (2). In the drybox 141 mg (0.183 mmol) of **1** and ca. 3 mL of C_6H_6 were added to a glass bomb. The reaction vessel was sealed and transferred to a vacuum line and 0.37 mmol of PMe_3 was added via vacuum transfer. The reaction mixture was heated to 45 °C for 14 h during which time it turned from orange to dark red. The volatile materials were removed in vacuo leaving a dark red residue that was taken into the drybox. The residue was taken up into hexane and this solution was cooled to −40 °C in the freezer giving 98

Table X. Crystal and Data Collection Parameters for **1**

A) Crystal Parameters at T = -45±5°C [a]

a = 11.3383 (27)Å	Space Group $P\bar{1}$
b = 14.3940 (20) Å	Formula Weight = 772.03 amu
c = 16.7212(27) Å	Z = 4
α = 92.668 (12) °	d_c = 1.96 g cm^{-3}
β = 92.351 (17) °	μ (calc.) = 101.3 cm^{-1}
γ = 105.783 (16) °	
V = 2619.1(17) Å^3	

Size of crystal: 0.32 x 0.32 x 0.35mm

B) Data Measurements Parameters (B)
Radiation Mo Kα (λ = 0 70926 Å)
Monochromator. Htghly-oriented graphite (2Θ =12.2°)
Detector Crystal scintillatton counter, with PHA.
Reflections measured: -h, ±k, ±L
2Θ Range: 3° -> 45° Scan Type: Θ-2Θ
Scan speed 0 72 -> 6 7 (Θ, °/mtn)
Scan width: $\Delta\Theta$ = 0.6 + 0 347 tan (Θ)
Background: Measured over 0 25 ($\Delta\Theta$) added to each end of the scan.
Aperture -> crystal = 173.0 mm Vertical aperture = 3.0 mm
Horizontal aperture = 2.4 + 1 0 tan(Θ) mm (variable)
No. of unique reflections collecled: 6811
Intensity standards. (820), (093), (1 3.1): measured every hour of x-ray exposure time. Over the data collection period no decrease in intenstty was observed.
Orientatton: 3 reflections were checked after every 200 measurements. Crystal orientation was redetermined if any of the reflections were offset from their predicted positions by more than 0.1°. Reorientation was not needed during data collection

[a] Unit cell parameters and their esd's were derived by a least-squares fit to the setting angles of the unresolved Mo Kα components of 24 reflections with 2Θ near 28°.

(28) For a description of the X-ray diffraction and analysis protocols used, see: (a) Hersh, W. H.; Hollander, F. J.; Bergman, R. G. *J. Am. Chem. Soc.* **1983**, *105*, 5834. (b) Roof, R. B., Jr. *A Theoretical Extension of the Reduced-Cell Concept in Crystallography*; Publication LA-4038, Los Alamos Scientific Laboratory: Los Alamos, NM 1969. (c) Cromer, D. T.; Waber, J. T. *International Tables for X-ray Crystallography*; Kynoch Press: Birmingham, England, 1974; Vol. IV, Table 2.2B.

Table XI. Crystal and Data Collection Parameters for **2**

A) Crystal Parameters at T = 25 °C

a = 17.1997 (20)Å	Space Group: P2(1)/n
b = 8.7132 (9) Å	Formula Weight = 771.0 amu
c = 18.2611 (21) Å	Z = 4
α = 90.000 (0) deg	d_c = 1.94 g cm^{-3}
β = 106.362 (10) °	μ (calc.) = 101.1 cm^{-1}
γ = 90.000 (0) °	
V = 2637.6 (10) Å3	
Size: 0.14 x 0.15 x 0.31mm	

B) Data Measurement Parameters (B)
Radiation: Mo Kα (λ = 0.71073 Å)
Monochromator: Highly-oriented graphite (2Θ =12.2°)
Detector: Crystal scintillation counter, with PHA.
Reflections measured: +H, +K, ±L
2Θ Range: 3 -> 45° Scan Type: Θ-2Θ
Scan speed: 0.72 -> 6.7 (Θ, °/min)
Scan width: ΔΘ = 0.6 + 0.347 tan (Θ)
Background: Measured over 0.25 (scan width) added to each end of the scan.
Vertical aperture = 3 mm Horizontal aperture = 2.0 + 1.0 tan(Θ) mm
No. of reflections collected: 3853
No. of unique reflections: 3447
Intensity standards: (6.5, -4), (3, 2, -12), (10, 2, -3): measured every one hour of X-ray exposure time. Over the data collection period a 5.2% decrease in intensity was observed.
Orientation: 3 reflections were checked after every 200 measurements. Crystal orientation was redetermined if any of the reflections were offset by more than 0.10 ° from their predicted positions. Reorientation was performed once during data collection.

mg (0.127 mmol, 70%) of **2** as dark red, analytically pure crystals. IR (KBr) 2971 (s), 2910 (s), 1455 (m), 1379 (s), 1296 (m), 1150 (br s), 1030 (m), 945 (s); ^{1}H NMR (C_6D_6) δ 7.94 (dd, J = 5.1, 16.7 Hz, 1 H), 5.52 (q, J = 5.3 Hz, 1 H), 2.15 (d, J = 5.6 Hz, 1 H), 1.93 (d, J = 1.8 Hz, 15 H), 1.90 (s, 15 H), 1.34 (d, J = 9.3 Hz, 9 H), 1.18 (d, J = 6.4 Hz, 1 H); ^{13}C NMR (C_6D_6) δ 107.7 (dd, J_{CP} = 9.5 Hz, J_{CH} = 151 Hz), 91.2 (d, J_{CP} = 2 Hz), 86.7 (s), 76.8 (d, J = 158 Hz), 29.5 (t, J = 151 Hz), 19.4 (dq, J_{CP} = 34.6 Hz, J_{CH} = 127.5 Hz), 12.05 (q, J = 126 Hz), 11.53 (q, J = 126 Hz); ^{31}P{^{1}H} NMR (C_6D_6) δ −39.4; MS, m/e 770, 694 (M^+, base); UV (hexane) λ_{max} 276 (ε = 1.6 × 10^4), 341 (ε = 8.8 × 10^3), 500 (ε = 4.2 × 10^3). Anal. Calcd for $C_{26}H_{43}Ir_2P$: C, 40.52; H, 5.58. Found: C, 40.48; H, 5.69.

Single-Crystal X-ray Diffraction Study of 2. Red, platelike crystals of **2** were obtained by slow evaporation of diethyl ether from a diethyl ether/acetonitrile solution at room temperature in the drybox. Some of these crystals were mounted in thin-wall glass cpaillaries in the air. The capillaries were then flushed with dry nitrogen and flame-sealed. Preliminary precision photographs indicated monoclinic Laue symmetry and yielded approximate cell dimensions.

The crystal used for data collection was then transferred to our Enraf-Nonius CAD-4 diffractometer and centered in the beam.[28] Automatic peak search and indexing procedures yielded the same monoclinic reduced primitive cell. The final cell parameters and specific data collection parameters for this data set are given in Table XI.

The 3853 raw intensity data were converted to structure factor amplitudes and their esds by correction for scan speed, background, and Lorentz and polarization effects. Inspection of the intensity standards revealed a reduction of 5.2% of the original intensity. The data were corrected for this decay. Inspection of the azimuthal scan data shoed a variation I_{min}/I_{max} = 0.71 for the average curve. An absorption correction based on the measured shape and size of the crystal and a 16 × 8 × 16 Gaussian grid of internal points was applied to the data (T_{max} = 0.366, T_{min} = 0.247). Inspection of the systematic absences indicated uniquely spaced group $P2_1/n$. Removal of systematically absent and redundant data left 3447 unique data in the final set.

The structure was solved by Patterson methods and refined via standard least-squares and Fourier techniques. In a difference Fourier map calculated following the refinement of all non-hydrogen atoms with anisotropic thermal parameters, peaks were found corresponding to possible positions of two iridium atoms of the other enantiomer of the molecule. These were included and refined with isotropic thermal parameters and their occupancy was adjusted to 0.04 to make them approximately the same as their high-occupancy equivalents. Further difference fourier maps suggested the position of a 4% occupancy position for phosphorus and indicated the disorder of the methyl carbon atoms on Cp2. These disordered atoms were included in structure factor calculations but were not refined. In the final difference Fourier map, indications of possible positions for the allyl hydrogens were seen, but they were not convincing.

The final residuals for 271 variables refined against the 2838 data for which $F^2 > 3\sigma(F^2)$ were R = 2.50%, wR = 3.61%, and GOF = 1.756. The R value for all 3447 data was 4.6%. In the final cycles of refinement a secondary extinction parameter was included, which gave a 10% correction to the most intense reflections.

The quantity minimized by the least-squares program was $\sum w(|F_o| - |F_c|)^2$, where w is the weight of a given observation. The p factor used to reduce the weight of intense reflections was set to 0.03 throughout the refinement. The analytical forms of the scattering factor tables for the neutral atoms were used and all scattering factors were corrected for both the real and imaginary components of anomalous dispersion.

Inspection of the residuals ordered in ranges of sin (Θ)/λ, $|F_o|$, and parity and value of the individual indexes showed no unusual features or trends. The largest peak in the final difference Fourier map had an electron density of 0.55 e$^-$/Å^3, and the lowest excursion −0.47 e$^-$/Å^3. Selected bond distances and angles are given in Tables III and IV. The positional and thermal parameters of the atoms, along with a listing of the values of F_o and F_c, are available as supplementary material.

ORTEP diagrams for **2** are shown in Figures 2 and 3. There are no abnormally short contacts between molecules. In each molecule one Ir atom is σ-bonded to a phosphorus and to C1 of the allyl group. The other Ir is π-bonded to the allyl. Each Ir atom has its coordination sphere filled out by a (η^5-C_5Me_5) ligand and there is a presumed Ir–Ir bond.

The only unusual thing about the structure is the disorder. In approximately 4% of the sites, a molecule of the enantiomer of the molecule shown, which normally sits elsewhere in the unit cell, occupies the site. Ir2′ is equivalent to Ir1 and Ir1′ to Ir2. The reason that this does not disrupt the crystal structure is easily seen from the distances and angles tables and from Figure 3. Even with the shift of the Ir atoms, and the phosphorus, the Cp′ rings do not have to shift an appreciable distance, nor do C1 and C3 of the allyl group and two of the three methyl groups of the PMe_3 moiety.

The extent of the disorder was estimated by refining the Ir atoms and adjusting their occupancy unitl their thermal parameters were equivalent to those of the majority occupant of the site. The phosphorus was not refined because, although it was detectable, refining it would have been equivalent to refining a partial hydrogen atom. At the 4% level it was not possible to detect partial carbon atoms. Due to the fact that the minority component Ir atoms are well-separated from the majority component, the disorder has little or no effect on the distances and angles calculated.

(η^5-C_5Me_5)(CO)Ir(η^1,η^3-C_3H_4)Ir(η^5-C_5Me_5) (3). In the drybox a solution of **1** (50 mg, 0.065 mmol) in ca. 3 mL of benzene was added to a glass bomb. The reaction vessel was sealed and removed to a vacuum line and the solution was degassed. At room temperature 430 Torr of CO was added above the solution. The resulting mixture was heated to 45 °C for 30 h after which time the volatile materials were removed in vacuo, leaving an orange residue. The residue was dissolved in hexane and upon cooling to −40 °C in the drybox freezer 30 mg (0.042 mmol) of analytically pure, orange crystals of **3** were formed (64% yield). IR (KBr) 2980 (s), 2914 (s), 2010 (w), 1935 (s), 1555 (br m), 1380 (s), 1275 (m), 1039 (m), 570 (m), 510 (m); ^{1}H NMR (C_6D_6) δ 8.16 (dt, J = 4.9, 1.1 Hz, 1 H), 5.64 (m, 1 H), 2.38 (dt, J = 5.4, 1.2 Hz, 1 H), 1.97 (s, 15 H), 1.90 (s, 15 H), 1.38 (dt, J = 6.3, 1.2 Hz, 1 H); ^{13}C NMR (C_6D_6) δ 174.8 (s), 97.5 (d, J = 161.3 Hz), 95.5 (s), 88.2 (s), 79.5 (d, J = 159.2 Hz), 27.6 (t, J = 159.2 Hz), 11.2 (q, J = 127 Hz), 10.8 (q, J = 126.5 Hz); MS, m/e 722, 694 (M^+, base); UV (hexane) λ_{max} 263 (ε = 1 × 10^4), 326 (ε = 8.5 × 10^3), 383 (ε = 3.4 × 10^3), 454 (ε = 3 × 10^3). Anal. Calcd for $C_{24}H_{34}Ir_2O$: C, 39.87; H, 4.71. Found: C, 39.80; H, 4.74.

(η^5-C_5Me_5)(η^2-CH_2=CH_2)Ir(η^1,η^3-C_3H_4)Ir(η^5-C_5Me_5) (4). In the drybox a solution of **1** (52 mg, 0.068 mmol) in ca. 3 mL of benzene was added to a glass bomb. The reaction vessel was sealed with a Kontes vacuum stopcock and the reaction vessel was removed to the vacuum line. The solution was degassed and 0.80 mmol of ethylene was added to the solution via vacuum transfer. The reaction materials were heated to 45 °C for 22 h after which the volatile materials were removed in vacuo. The orange residue was dissolved in pentane and then cooled to −40 °C in the drybox freezer, giving 24 mg of **4** (0.033 mmol; 49% yield) as an orange, analytically pure powder. IR (KBr) 2977 (s), 2904 (s), 1473 (br m), 1379 (s), 1284 (m), 1158 (s), 1027 (m), 579 (m); ^{1}H NMR (C_6D_6) δ 7.12 (d, J = 5 Hz, 1 H), 5.32 (m, 1 H), 2.28 (d, J = 5.4 Hz, 1 H), 1.83 (s, 15 H), 1.78 (s, 15 H), 1.28 (d, J = 6.3 Hz, 1 H), 1.09–1.15 and 1.6–1.85 (m, 4 H); ^{13}C NMR (C_6D_6) δ 119.9 (d, J = 152.7 Hz), 92.7 (s), 87.4 (s), 78.2 (t, J = 160.5 Hz), 31.3 (t, J = 151.4 Hz), 24.5 (t, J = 153.1 Hz), 18.0 (t, J = 152 Hz), 10.8 (q, J = 126.3 Hz; exactly overlapping methyl resonances for the two η^5-C_5Me_5 ligands), 10.4 (q, J = 126.6 Hz); MS, m/e 722, 694 (M^+, $M^+ - C_2H_4$ base); UV (hexane) λ_{max} 273 (ε = 1 × 10^4), 328 (ε = 1 × 10^4), 474 (ε = 3.1 × 10^3). Anal. Calcd for $C_{25}H_{38}Ir_2$: C, 41.53; H, 5.26. Found: C, 41.39; H, 5.36.

(η^5-C_5Me_5)P(OCH_3)$_3$Ir(η^1,η^3-C_3H_4)Ir(η^5-C_5Me_5) (5). In the drybox a solution of **1** (40 mg, 0.052 mmol) in ca. 2 mL of hexane was added to a glass bomb. The bomb was sealed and then removed to the vacuum

line. The solution was degassed and 0.25 mmol of $P(OCH_3)_3$ was added to the solution via vacuum transfer. The reaction materials were heated to 45 °C for 7 h after which the volatile materials were removed in vacuo leaving a red residue. This residue was dissolved in hexane and upon cooling to −40 °C in the drybox freezer 38 mg (0.046 mmol; 89% yield) of **5** was collected as red, analytically pure crystals. IR (KBr) 2968 (s), 2946 (s), 2987 (s), 1453 (br, m), 1377 (s), 1054 (s), 1030 (s), 741 (s), 574 (m); ^1H NMR (C_1D_6) δ 8.15 (dd, J = 5, 13.5 Hz, 1 H), 5.51 (m, 1 H), 3.38 (d, J = 11.4 Hz, 9 H), 2.23 (d, J = 5.2 Hz, 1 H), 1.99 (s, 15 H), 1.98 (d, J = 3 Hz, 15 H), 1.26 (d, J = 6.3 Hz, 1 H); ^{13}C NMR (C_6D_6) δ 106.1 (dd, J_{CP} = 18.4 Hz, J_{CH} = 158 Hz), 92.9 (d, J_{CP} = 4.7 Hz), 87.4 (s), 77.3 (d, J = 158 Hz), 51.7 (dq, J_{CP} = 5.7 Hz, J_{CH} = 144 Hz), 28.8 (t, J = 153 Hz), 11.7 (q, J = 126 Hz), 11.2 (q, J = 126 Hz); $^{31}P\{^1H\}$ NMR (C_6D_6) δ 92.1; MS, m/e 818 (M^+ base); UV (hexane) λ_{max} 265 ($\epsilon = 1.3 \times 10^4$), 331 ($\epsilon = 1.1 \times 10^4$), 484 ($\epsilon = 3.6 \times 10^3$). Anal. Calcd for $C_{26}H_{43}Ir_2PO_3$: C, 38.12; H, 5.25. Found: C, 38.05; H, 5.40.

(η^5-C_5Me_5)(t-BuNC)Ir(η^1,η^3-C_3H_4)Ir(η^5-C_5Me_5) (6). In the drybox a solution of **1** (50 mg, 0.065 mmol) in hexane (ca. 3 mL) was added to a glass bomb. The bomb was sealed and transferred to a vacuum line and the solution degassed. On the vacuum line 0.30 mmol of t-BuNC was added to the solution of **1** and the resulting reaction mixture was heated to 45 °C for 14 h. The volatile materials were removed in vacuo, leaving an orange residue. Crystallization from hexane at −40 °C in the drybox freezer gave **6** in 61% yield (31 mg, 0.040 mmol) as orange analytically pure crystals. IR (KBr) 2972 (s), 2902 (s), 1898 (br s, CN), 1472 (m), 1456 (m), 1378 (s), 1363 (m), 1202 (s), 1031 (m); ^1H NMR (C_6D_6) δ 8.21 (dt, J = 4.9, 1 Hz, 1 H), 5.65 (m, 1 H), 2.40 (dt, J = 5.3, 1 Hz, 1 H), 2.09 (s, 15 H), 1.99 (s, 15 H), 1.29 (s, 9 H), 1.26 (dt, J = 6.3, 1 Hz, 1 H); $^{13}C\{^1H\}$ NMR (C_6D_6) δ 169.2 (s), 102.0 (s), 93.7 (s), 87.5 (s), 78.7 (s), 52.5 (s), 32.6 (s), 27.1 (s), 11.4 (s), 11.2 (s); MS, m/e 777, 44 (M^+, base); UV (hexane) λ_{max} 256 ($\epsilon = 1.4 \times 10^4$), 331 ($\epsilon = 9 \times 10^3$, shoulder at ca. 381), 464 ($\epsilon = 4.1 \times 10^3$). Anal. Calcd for $C_{28}H_{43}Ir_2N$: C, 43.22; H, 5.53; N, 1.80. Found: C, 43.62; H, 5.76; N, 1.80.

Irradiation of CO and Ethylene Complexes 3 and 4 in Benzene. In the drybox an NMR tube sealed to a glass joint was charged with 6 mg (0.008 mmol) of the CO complex **3**, 3 mg of ferrocene (as an internal standard), and 0.6 mL of C_6D_6. The NMR tube was fitted to a Kontes vacuum stopcock and the apparatus was transferred to the vacuum line. The solution was degassed and then the NMR tube was flame sealed under vacuum. The reaction was monitored by ^1H NMR analysis. Irradiation for 44 h produced 89% conversion of **3** and a 54% yield of **1**-d_6. The above procedure was repeated, giving a 42% yield. Analogous procedures utilizing the ethylene complex **4** yielded 53% and 40% yields of **1**-d_6.

Thermolysis of 2: Isolation of (η^5-C_5Me_5)(H)Ir(η^1,η^1-Me_2PCH_2)(η^1,η^3-C_3H_4)Ir(η^5-C_5Me_5) (7). In the drybox a glass bomb was charged with 82 mg (0.106 mmol) of the phosphine complex **2** and ca. 3 mL of C_6H_6. The reaction vessel was sealed and transferred to a vacuum line and the solution degassed. The reaction mixture was heated to 100 °C for 11.5 h during which time the dark red solution lightened to a pale orange. The volatile materials were removed in vacuo and a ^1H NMR spectrum of the residue was taken showing the clean production of two new complexes in a 10:1 ratio. The residue was purified by extraction into hexane followed by two crystallizations at −40 °C in the drybox freezer, giving 43 mg (0.056 mmol, 52%) of the major product, **7**, as analytically pure, light yellow crystals. IR (KBr) 2970 (s), 2910 (s), 2860 (s), 2120 (s, Ir-H), 1450 (br m), 1380 (s), 1270 (s), 1035 (s), 905 (s); ^1H NMR (C_1D_6) δ 4.46 (d, J = 7.1 Hz, 1 H), 4.01 (q, J = 7.2 Hz, 1 H), 2.63 (d, J = 5.7 Hz, 1 H), 2.47 (t, J = 11.3 Hz, 1 H), 1.97 (d, J = 1.3 Hz, 15 H), 1.81 (d, J = 5.7 Hz, 1 H), 1.64 (d, J = 8.6 Hz, 3 H), 1.63 (s, 15 H), 1.45 (dd, J = 4.8, 11.3 Hz, 1 H), 1.12 (d, J = 9.8 Hz, 3 H), −18.1 (d, J = 37.7 Hz, 1 H); ^{13}C NMR (C_6D_6) δ 91.2 (d, J_{CP} = 3 Hz), 89.3 (s), 82.4 (d, J = 153.3 Hz), 42.4 (dd, J_{CP} = 11.9 Hz, J_{CH} = 136.5 Hz), 39.0 (t, J = 153.7 Hz), 20.8 (dq, J_{CP} = 24.5 Hz, J_{CH} = 126.2 Hz), 18.3 (dt, J_{CP} = 33.4 Hz, J_{CH} = 125.6 Hz), 15.2 (dq, J_{CP} = 31.8 Hz, J_{CH} = 123 Hz), 10.3 (q, J = 126.2 Hz), 9.2 (q, J = 126.6 Hz); $^{31}P\{^1H\}$ NMR (C_6D_6) δ 35.1; MS, m/e 770, 694 (M^+, base); UV (hexane) λ_{max} 270 ($\epsilon = 8 \times 10^3$). Anal. Calcd for $C_{26}H_{43}Ir_2P$: C, 40.52; H, 5.58. Found: C, 40.59; H, 5.65.

Single-Crystal X-ray Diffraction Study of 7. Clear, yellow prismatic crystals of the compound were obtained by slow crystallization from a diethyl ether/acetonitrile mixture. Some of these crystals were mounted on glass fibers with polycyanoacrylate cement. Preliminary precession photographs indicated monoclinic Laue symmetry and yielded approximate cell dimensions.

The crystal used for data collection was then transferred to our Enraf-Nonius CAD-4 diffractometer[28] and centered in the beam. Automatic peak search and indexing procedures yielded a monoclinic reduced primitive cell. Inspection of the Niggli values[28b] revealed no conventional cell of higher symmetry. The final cell parameters and specific data collection parameters for this data set are given in Table XII.

Table XII. Crystal and Data Collection Parameters for **7**

A) Crystal Parameters at T = 25 °C

a = 7.5575 (12)Å	Space Group: P2(1)/n
b = 22.663 (4) Å	Formula Weight = 771.0 amu
c = 15.6449 (16) Å	Z = 4
α = 90.000 (0) deg	d_c = 1.92 g cm^{-3}
β = 94 968 (11) °	μ (calc.) = 99.9 cm^{-1}
γ = 90.000 °	
V = 2669.5 (12) Å^3	
Size: 0.16 x 0.17 x 0.29 mm	

B) Data Measurement Parameters (B)

Radiation: Mo Kα (λ = 0.71073 Å)
Monochromator: Highly-oriented graphite (2Θ =12.2°)
Detector: Crystal scintillation counter, with PHA.
Reflections measured: +H, +K, ±L
2Θ Range: 3 -> 45° Scan Type: Θ-2Θ
Scan speed: 0.90 -> 6.7 (Θ, °/mtn)
Scan width: ΔΘ = 0.75 + 0.35 tan (Θ)
Background: Measured over 0.25 (scan width) added to each end of the scan.
Vertical aperture = 4.0 mm Horizontal aperture = 2.5 + 1.0 tan(Θ) mm
No. of reflections collected: 3602
No. of unique reflections: 3483
Intensity standards: (5, 0, 1), (2, 13, -3), (2, 4, 9): measured every one hour of x-ray exposure time. Over the data collection period a 16% decrease in intensity was observed
Orientation: 3 reflections were checked after every 200 measurements. Crystal orientation was redetermined if any of the reflections were offset by more than 0.10 ° from their predicted positions. Reorientation was performed 2 times during data collection.

The 3602 raw intensity data were converted to structure factor amplitudes and their esds by correction for scan speed, background, and Lorentz and polarization effects. Inspection of the intensity standards revealed an overall reduction of 16% of the original intensity. The data were corrected for this decay. Inspection of the azimuthal scan data showed a variation I_{min}/I_{max} = 0.46 for the average curve. An absorption correction based on the measured shape and size of the crystal and a 14 × 14 × 8 Gaussian grid of internal points was applied to the data (T_{max} = 0.254, T_{min} = 0.083). Inspection of the systematic absences indicated uniquely space group $P2_1/n$. Removal of systematically absent and redundant data left 3483 unique data in the final data set.

The structure was solved by Patterson methods and refined via standard least-squares and Fourier techniques.[28] There was no indication of hydrogen atoms in the final difference Fourier map and they were not included in structure factor calculations.

The final residuals for 263 variables refined against the 2775 data for which $F^2 > 3\sigma F^2$ were R = 4.38%, wR = 5.84%, and GOF = 2.74. The R value for all 3483 data was 7.4%. In the final cycles of refinement a secondary extinction parameter was included.

The quantity minimized by the least-squares program was $\sum w(|F_o| - |F_c|)^2$, where w is the weight of a given observation. The p factor, used to reduce the weight of intense reflections, was set to 0.03 throughout the refinement. The analytical forms of the scattering factor tables for the neutral atoms were used and all scattering factors were corrected for both the real and imaginary components of anomalous dispersion.[28c]

Inspection of the residuals ordered in ranges of sin (Θ)/λ, F_o, and parity and value of the individual indexes showed no unusual features or trends. The largest peak in the final difference Fourier map had an electron density of 2.77 e$^-$/Å^3, and the lowest excursion −1.17 e$^-$/Å^3. Both were located near the iridium atoms. An ORTEP diagram of the molecule is shown in Figure 4; selected distances and angles are given in Tables V and VI. The positional and thermal parameters for the atoms, along with a listing of F_o and F_c, are provided as supplementary material.

(η^5-C_5Me_5)(η^2-Me_2P=CH_2)Ir(η^1,η^2-CH=$CHCH_3$)Ir(η^5-C_5Me_5) (8). In the drybox a glass bomb was charged with 61 mg (0.079 mmol) of the PMe_3 complex **2** and ca. 2 mL of C_6H_6. The bomb was sealed and removed to the vacuum line and the solution was degassed. After heating to 100 °C for 13 days, the solution had turned from dark red to bright orange. The volatile materials were removed in vacuo and the resulting orange residue was dissolved in hexane; upon cooling to −40 °C in the drybox freezer, 34 mg (0.044 mmol, 56%) of air-sensitive, analytically pure orange crystals of **8** were isolated. ^1H NMR (C_6D_6) δ 7.15 (d, J = 8.3 Hz, 1 H), 2.40 (m, 1 H), 1.92 (s, 15 H), 1.78 (narrow multiplet containing resonances due to one η^5-C_5Me_5 ligand and the vinyl methyl group; integration approximately 18 H), 1.60 (d, J = 10.5 Hz, 3 H), 1.18 (d, J = 8.1 Hz, 3 H), 0.30 (dd, J = 4.3, 10.2 Hz, 1 H), −0.04 (dd, J = 8, 10.3 Hz, 1 H); ^1H NMR (CD_2Cl_2) δ 6.80 (d, J = 8.9 Hz, 1 H), 2.41 (m, 1 H), 1.89 (d, J = 1.9 Hz, 15 H), 1.84 (s, 15 H), 1.65 (d, J = 10.6

Hz, 3 H), 1.55 (d, J = 5.9 Hz, 3 H), 1.16 (d, J = 8.3 Hz, 3 H), −0.31 (m, 2 H); ^{13}C NMR (C_6D_6) δ 107.3 (d, J = 140 Hz), 91.1 (s), 85.1 (s), 41.7 (d, J = 152 Hz), 24.2 (q, J = 127.5 Hz), 22.4 (q, J = 127 Hz), 19.7 (dq, J_{CP} = 50.2 Hz, J_{CH} = 125 Hz), 10.8 (q, J = 126 Hz), 10.6 (q, J = 126 Hz), −23.5 (dt, J_{CP} = 22.6 Hz, J_{CH} = 136 Hz); ^{31}P{^{1}H} NMR (C_6D_6) δ −89.5; MS, m/e 770 (M^+ base); UV (hexane) λ_{max} 416. Anal. Calcd for $C_{26}H_{43}Ir_2P$: C, 40.50; H, 5.58. Found: C, 40.35; H, 5.66.

Thermolysis of 4: $(\eta^5\text{-}C_5Me_5)Ir(\eta^1,\eta^2\text{-}C_3H_5)(\eta^2,\eta^1\text{-}C_2H_3)Ir(\eta^5\text{-}C_5Me_5)$ (9). In the drybox a hexane solution (2 mL) of the ethylene complex **4** (35 mg, 0.048 mmol) was added to a glass bomb. The bomb was sealed and transferred to the vacuum line and the solution degassed. After heating the solution to 100 °C for 7 h, the volatile materials were removed in vacuo. The resulting yellow-orange residue was dissolved in hexane and upon cooling to −40 °C in the drybox freezer 29 mg (0.040 mmol, 83%) of analytically pure, orange crystals of **9** formed. ^{1}H NMR (C_6D_6) δ 7.38 (dd, J = 7.1, 9.1 Hz, 1 H), 3.40 (dd, J = 0.8, 7.1 Hz, 1 H), 2.85 (m, 1 H), 2.30 (t, J = 8 Hz, 1 H), 2.23 (d, J = 9.2 Hz, 1 H), 1.90 (t, J = 6.4 Hz, 1 H), 1.74 (s, 15 H), 1.70 (s, 15 H), 1.25 (d, J = 7.8 Hz, 1 H), 0.56 (d, J = 10.3 Hz, 1 H); ^{13}C NMR (C_6D_6) δ 111.2 (d, J = 149.3 Hz), 91.6 (s), 90.2 (s), 44.2 (dd, J = 146, 159 Hz), 34.8 (d, J = 153.5 Hz), 30.9 (t, J = 157 Hz), 9.9 (q, J = 126 Hz), −14.1 (t, J = 134 Hz); MS, m/e 722 (M^+ base); UV (hexane) λ_{max} 414. Anal. Calcd for $C_{25}H_{38}Ir_2$: C, 41.53; H, 5.26. Found: C, 41.80; H, 5.56.

$(\eta^5\text{-}C_5Me_5)(H)Ir(\mu\text{-}H)(\eta^1,\eta^3\text{-}C_3H_4)Ir(\eta^5\text{-}C_5Me_5)$ (10). In the drybox a glass bomb was charged with 75 mg (0.097 mmol) of **1** and ca. 3 mL of pentane. The reaction vessel was sealed and removed to a vacuum line and the solution degassed. At room temperature, on the vacuum line, 600 Torr of H_2 was added above the reaction mixture. The reaction mixture was heated to 50 °C for 15 h after which the volatile materials were removed in vacuo leaving an orange residue. The residue was dissolved in hexane and upon cooling to −40 °C in the drybox freezer orange, analytically pure crystals of the dihydride complex **10** formed (54 mg, 0.078 mmol, 80% yield). IR (KBr) 2990 (s), 2905 (br s), 2085 (s, Ir-H), 1450 (br s), 1380 (s), 1280 (s), 1030 (s), 860 (s); ^{1}H NMR (C_6D_6) δ 7.89 (d, J = 5.6 Hz, 1 H), 4.90 (m, 1 H), 2.09 (s, 15 H), 1.99 (d, J = 5.4 Hz, 1 H), 1.75 (s, 15 H), 1.18 (br d, J = 7.3 Hz, 1 H), −18.28 (s, 1 H), −18.47 (s, 1 H); ^{1}H NMR (C_6D_{12}) δ 7.56 (d, J = 5.6 Hz, 1 H), 4.66 (m, 1 H), 2.01 (s, 15 H), 1.94 (s, 15 H), 1.68 (d, J = 5.6 H, 1 H), 0.59 (dd, J = 2.6, 7.3 Hz, 1 H), −18.51 (s, 1 H), −19.25 (s, 1 H); ^{13}C{^{1}H} NMR (C_6D_6) δ 106.5 (s), 90.2 (s), 88.8 (s), 81.5 (s), 41.7 (s), 11.6 (s), 10.6 (s); MS, m/e 696 (M^+ base); UV (hexane) λ_{max} 250 ($\epsilon = 1.3 \times 10^4$), 335 ($\epsilon = 4 \times 10^3$), 468 ($\epsilon = 1.3 \times 10^3$). Anal. Calcd for $C_{23}H_{36}Ir_2$: C, 39.63; H, 5.58. Found: C, 39.74; H, 5.32.

$(\eta^5\text{-}C_5Me_5)(CH_2CN)Ir(\mu\text{-}H)(\eta^1,\eta^3\text{-}C_3H_4)Ir(\eta^5\text{-}C_5Me_5)$ (11). In the drybox 58 mg (0.075 mmol) of **1** was dissolved in 5 mL of THF and this orange solution was added to a glass bomb, to which was added 0.5 mL of acetonitrile. The bomb was sealed with a Kontes vacuum stopcock and the reaction vessel was removed to a vacuum line. The solution was degassed and heated to 50 °C for 30 h. The volatile materials were removed in vacuo, leaving an orange residue that was dissolved in hexane. The hexane solution was cooled to −40 °C in the drybox freezer, giving 37 mg (0.050 mmol, 67%) of orange, analytically pure crystals of **11**. IR (KBr) 2990 (s), 2910 (br s), 2195 (sh s, CN), 1460 (br m), 1385 (s), 1280 (s), 1039 (s), 895 (s); ^{1}H NMR (C_6D_6) δ 7.38 (d, J = 5.4 Hz, 1 H), 5.33 (m, 1 H), 1.99 (d, J = 5.5 Hz, 1 H), 1.84 (s, 15 H), 1.69 (s, 15 H), 1.50 (d, J = 14.2 Hz, 1 H), 1.19 (br d, J = 8.2 Hz, 1 H), 1.10 (d, J = 14.2 Hz, 1 H), −21.0 (s, 1 H); ^{13}C NMR (C_6D_6) δ 130.8 (t, J = 7.3 Hz), 104.7 (d, J = 149 Hz), 90.4 (s), 89.2 (s), 84.7 (d, J = 157.1 Hz), 30.6 (t, J = 156.2 Hz), 10.2 (q, J = 127.5 Hz), 9.7 (q, J = 127.1 Hz), −29.7 (t, J = 136.8 Hz); MS, m/e 735, 69 (M^+, base); UV (hexane) λ_{max} 236 ($\epsilon = 1.2 \times 10^4$), 340 ($\epsilon = 3.7 \times 10^3$), 438 ($\epsilon$ = 770). Anal. Calcd for $C_{25}H_{37}Ir_2N$: C, 40.79; H, 5.03; N, 1.90. Found: C, 41.01; H, 5.15; N, 1.86.

Rate Studies on Dinuclear Reductive Elimination of Benzene from 1 by ^{1}H NMR Spectrometry. Into an NMR tube, which was fused to a glass joint, was charged 9 mg (0.012 mmol) of **1** followed by the addition of 0.6 mL of C_6D_{12} and $(Me_3Si)_2O$ as an internal standard. A Kontes vacuum stopcock was attached to the NMR tube apparatus, after which it was removed to the vacuum line and the solution degassed. To the reaction mixture was added $P(OCH_3)_3$ (0.065 mmol) via vacuum transfer, and the tube was then sealed under vacuum. The reaction was followed by monitoring the decrease in the integration of the (η^5-C_5Me_5) methyl resonance in the ^{1}H NMR spectrum through 3 half-lives at 45 °C; clean first-order disappearance of **1** was observed; $k_{obs} = 1.65 \times 10^{-4}$.

Rate Studies by UV Spectrometry. In the drybox a stock solution of **1** was made by dissolving 5.2 mg (0.0067 mmol) of **1** in 50 mL of hexane (1.35×10^{-4} M). A standard solution of PMe_3 was made by the addition of 0.74 mL of liquid PMe_3 to 20 mL of hexane using standard Schlenk techniques under argon. A typical UV kinetics experiment was performed by addition of 1 mL of the stock solution of **1** to a cuvette fitted with a rubber septum in the drybox using a volumetric pipet followed by the addition of the PMe_3 solution via syringe outside the drybox. The results of experiments run at various concentrations of **1** and PMe_3 at 50 °C are given in Table VII. Temperature-dependent rate constants are given in Table VIII.

Benzene/PMe_3 rate studies were performed as above with benzene as the solvent to circumvent solvent effects. The results of this study are given in Table IX.

Intermolecular Isotope Effect in Irradiation of 3 in C_6H_6/C_6D_6. In the drybox 12 mg (0.017 mmol) of the CO complex **3** was added to a glass bomb. To this was added 1.0 mL of C_6H_6 and 1.0 mL of C_6D_6. The bomb was sealed and removed to the vacuum line and the solution was degassed. The solution was irradiated at ca. 6 °C for 4 h, after which time an aliquot was removed in the drybox. The volatile materials were removed in vacuo, dissolved in C_6D_{12}, and analyzed by ^{1}H NMR spectroscopy. A calculated value for k_H/k_D(inter) = 1.51 was obtained by integration of the resulting m-aromatic proton resonance vs the β-allylic proton resonance. The remaining solution was irradiated for an additional 15 h. After workup a value of k_H/k_D(inter) = 1.58 was calculated. The above procedures were repeated 3 times, giving k_H/k_D(inter) = 1.54 ± 0.04.

To test the stability of the products in the photolysis reaction, a C_6D_6 solution of **1** was irradiated for 19 h, during which time no observable isotopic exchange occurred. Also, only a 9% reduction in starting material was observed by ^{1}H NMR spectrometry (mesitylene internal standard).

Intramolecular Isotope Effect. In the drybox 10 mg (0.014 mmol) of **3** was added to a glass bomb followed by the addition of 1 mL of 1,3,5-$C_6D_3H_3$. The bomb was sealed, removed to the vacuum line, and degassed. The solution was irradiated for 4 h and then worked up as described in the intermolecular case. A calculated value for k_H/k_D(intra) = 1.64 ± 0.15 was obtained by integration of the m-aromatic proton resonance vs the o-armatic proton resonance. After 24 h the calculated value was 1.63 ± 0.15.

Synthesis of 1-d_{10}: $(\eta^5\text{-}C_5Me_5)(C_6D_5)Ir(\mu\text{-}D)(\eta^1,\eta^3\text{-}C_3D_4)Ir(\eta^5\text{-}C_5Me_5)$. In the drybox a solution of $(\eta^5\text{-}C_5Me_5)Ir(\eta^3\text{-}C_3H_5)H$ (160 mg, 0.433 mmol) in C_6D_6 (5 mL) was added to a glass bomb. The bomb was sealed and removed to the vacuum line and the solution degassed. The reaction materials were heated to 50 °C for 17 h during which time the clear solution darkened.[23] After this period the solution was concentrated to ca. 1 mL in vacuo and the solution was heated to 50 °C for 6 d during which time the solution turned orange brown. The volatile materials were removed in vacuo leaving a dark orange-brown residue that was dissolved in hexane. Upon cooling to −40 °C in the drybox freezer orange crystals of **1**-d_{10} (40 mg, 0.051 mmol, 23%) formed. ^{1}H NMR (C_6D_6) δ 1.79 (s, 15 H), 1.53 (s, 15 H); ^{2}H{^{1}H} NMR (C_6H_6) δ 7.67 (br s), 5.22 (br s), 2.1 (br s), 1.21 (br s), −20.44 (s); MS, m/e 782, 698 (M^+, $M^+ - C_6D_6$ base).

Thermolysis of 1 in C_6D_6: Isotopic Exchange of Benzene. In the drybox 15 mg of **1** and 0.60 mL of C_6D_6 were added to an NMR tube, which was fused to a ground glass joint. The tube was fitted with a Kontes vacuum stopcock and removed to the vacuum line and the solution was degassed. The rate of isotopic exchange was monitored by ^{1}H NMR spectroscopy by observing the relative change in the o-aromatic proton resonance vs the α-allylic proton resonance. From this a value for $k_{obs} = 1.5 \times 10^{-4}$ was calculated.

Crossover Experiment: Thermolysis of 1 and 1-d_{10} with Added Ethylene. In the drybox a glass bomb was charged with 10 mg (0.013 mmol) of **1** and 10 mg (0.013 mmol) of **1**-d_{10} followed by the addition of 1 mL of pentane. The bomb was sealed and transferred to the vacuum line and the solution degassed. At room temperature 680 Torr of ethylene was added to the reaction mixture. The solution was heated to 50 °C for 2 h and 15 min after which time the volatile materials were transferred to a glass ampule on the vacuum line. The volatile materials were shown to be >90% C_6D_6 and C_6H_6 by GC mass spectrometry, with no indication of the crossover products, <10% C_6H_5D, C_6D_5H (limits given for uncertainty in measurements). The residue from the reaction was dissolved in C_6D_6 and by ^{1}H NMR analysis showed 95% reaction giving cleanly **4** and **4**-d_4 (η^1,η^3-C_3D_4).

Rate of Conversion of 2 to 7. In the drybox, to two separate NMR tubes fused to ground glass joints were added 5.5 mg (0.006 mmol) of **2**, 2 mg of ferrocene, and 0.6 mL of C_6D_6. To the NMR tubes were attached Kontes vacuum stopcocks, and the tubes were removed to the vacuum line and degassed. To one tube was added 0.024 mmol (0.4 M) of PMe_3 via vacuum transfer. The NMR tubes were flame sealed under vacuum and were then heated to 100 °C in an oil bath. By ^{1}H NMR spectroscopy rate constants were obtained for each reaction mixture: $k_{obs} = 1.33 \times 10^{-4}$; with added PMe_3, $k_{obs} = 1.22 \times 10^{-4}$.

$(\eta^5\text{-}C_5Me_5)P(CD_3)_3Ir(\eta^1,\eta^3\text{-}C_3H_4)Ir(\eta^5\text{-}C_5Me_5)$ (2-d_9). The procedures for the synthesis of **2**-d_9 were identical with those given for **2**. ^{1}H

NMR (C_6D_6) δ 2.14 (d, J = 5.2 Hz, 1 H), 1.93 (d, J_{HP} = 1.8 Hz, 15 H), 1.90 (s, 15 H), 1.18 (d, J = 6.4 Hz, 1 H); $^2H\{^1H\}$ NMR (C_6H_6) δ 1.29; $^{13}C\{^1H\}$ NMR (C_6D_6) δ 107.6 (d, J_{CP} = 9.8 Hz), 91.2 (d, J_{CP} = 2.6 Hz), 86.6 (s), 76.7 (s), 29.4 (s), 12.0 (s), 11.5 (s) (the phosphine carbons were not observed); $^{31}P\{^1H\}$ NMR (C_6D_6) δ −40.73 (s), −40.93;[29] MS, m/e 779 (M^+ base); UV (hexane) λ_{max} 266, 331, 500.

Thermolysis of 2-d_9. In the drybox 20 mg (0.026 mmol) of **2**-d_9 and 0.6 mL of C_6H_6 were added to an NMR tube that was fused to a ground glass joint. A Kontes vacuum stopcock was attached to the tube and the apparatus removed to the vacuum line and the solution degassed. The NMR tube was flame sealed under vacuum and the reaction mixture heated to 80 °C in an oil bath. After 4 h a new resonance appeared in the $^2H\{^1H\}$ NMR spectrum at δ 7.94 ppm. After an additional 4 h at 80 °C the NMR tube was cracked in the drybox, the volatile materials removed in vacuo, and then the residue dissolved in C_6D_6. ^1H NMR (C_6D_6) δ 5.53 (dt, J = 1.1, 6.5 Hz), 1.93 (d, J = 2 Hz), 1.90 (s), 1.29 (br d, J_{HP} = 9.4 Hz).[30]

The above product was again dissolved in C_6H_6 and heated to 100 °C for 4 h. New deuterium resonances in the $^2H\{^1H\}$ NMR spectrum appeared at δ 4.43, 2.39, 1.56, 1.05, −17.9 (d, J_{DP} = 5.7 Hz). After the solution was heated at 100 °C for an additional 4 h the solvent was once again changed to C_6D_6 and the ^1H NMR spectrum showed new proton resonances at δ 4.0 (br t, J = 6.7 Hz), 2.64 (d, J = 5.7 Hz), 1.64 (br s), 1.99 ns) for **7**-d_9.

(η^5-C_5Me_5)(η^2-CD_2=CD_2)Ir(η^1,η^3-C_3H_4)Ir(η^5-C_5Me_5) (**4**-d_4). The procedures for the synthesis of **4**-d_4 were identical with those given for **4**. ^1H NMR (C_6D_6) δ 7.10 (dt, J = 1, 5 Hz, 1 H), 5.28 (m, 1 H), 2.28 (br d, J = 5.4 Hz, 1 H), 1.83 (s, 15 H)8 1.77 (s, 15 H), 1.27 (d, J = 6.3 Hz); $^2H\{^1H\}$ NMR (C_6H_6) δ 1.6 (br s, 3D), 1.1 (br s, 1 D); MS, m/e 726, 694 (M^+, $M^+ - C_2D_4$ base).

Thermolysis of 4-d_4. A solution of **4**-d_4 in C_6D_6 was prepared in an NMR tube as described in the thermolysis of **2**-d_9 described above. The reaction materials were heated to 80 °C for 5 h, during which time no observable isotopic scrambling occurred by ^1H NMR spectrometry. Continued heating to 100 °C for 4 h and analysis by $^2H\{^1H\}$ NMR spectrometry in C_6H_6 showed the production of **9**-d_4. New resonances in the $^2H\{^1H\}$ NMR spectrum: δ 7.37, 3.34, 2.18 and broad peaks in the range 2-1 ppm.

Acknowledgment. This work was supported by the Director, Office of Energy Research, Office of Basic Energy Sciences, Chemical Sciences Division of the U.S. Department of Energy under Contract DE-AC03-76SF000098. W.D.M. acknowledges the Organic Division of the American Chemical Society for a predoctoral fellowship. We are also grateful for a generous loan of $IrCl_3 \cdot nH_2O$ from Johnson-Matthey, Inc., and for helpful discussions with Thomas Foo.

Registry No. 1, 103619-65-4; **1**-d_6, 116323-57-0; **1**-d_{10}, 116323-58-1; **2**, 103639-16-3; **2**-d_9, 116323-59-2; **3**, 103619-69-8; **4**, 103619-70-1; **4**-d_4, 116323-60-5; **5**, 103619-71-2; 6, 116323-61-6; **7**, 103619-66-5; **7**-d_9, 116323-62-7; **8**, 116323-63-8; **9**, 116323-64-9; **9**-d_4, 116323-65-0; **10**, 116323-66-1; **11**, 116323-67-2; (η^5-C_5Me_5)Ir(η^3-C_3H_5)H, 96427-40-6.

Supplementary Material Available: Tables of positional parameters and their estimated standard deviations, tables of general temperature factor expressions (B's), and root mean square amplitudes of thermal vibrations for **2** and **7** (10 pages); tables of F_o and F_c for the X-ray diffraction studies of complexes **2** and **7** (42 pages). Ordering information is given on any current masthead page. Full details of the X-ray diffraction study of complex **1** are given as supplementary material with the preliminary communication (ref 5c).

(29) We attribute the appearance of two resonances in the $^{31}P\{^1H\}$ NMR spectrum to be from **2**-d_9 and **2**-d_8; the difference in chemical shift is the result of slightly different isotopic perturbations on the phosphorous atom.

(30) This proton resonance corresponds to a small amount of hydrogen in the methyl groups of the phosphine ligand which originated from the α-allylic position in the starting material.

Reactive Iron Porphyrin Derivatives Related to the Catalytic Cycles of Cytochrome P-450 and Peroxidase. Studies of the Mechanism of Oxygen Activation

John T. Groves* and Yoshihito Watanabe†

Contribution from the Department of Chemistry, Princeton University, Princeton, New Jersey 08544. *Received March 14, 1988*

Abstract: The mechanism of oxidation of tetramesityliron(III) porphyrins [Fe^{III}TMP(X)] with peroxyacids has been examined. The reaction of Fe^{III}TMP(Cl) (**1**) with peroxyacids in methylene chloride at −46 °C afforded the corresponding oxoiron(IV) porphyrin cation radical [$Fe^{IV}TMP^{\cdot+}$(O)] (**3**). The kinetics of this process were complicated by an induction period that depended on the acidity of the peroxyacid used. By contrast, similar oxidation of Fe^{III}TMP(OH) gave evidence for rapid ligand metathesis to afford an acylperoxoiron(III) complex, Fe^{III}TMP(OOC(O)Ar) (**2**). The decomposition of **2** to form **3** was found to be first order in **2** and catalyzed by acid. Electron-withdrawing substituents on the aryl portion of the peroxyacid facilitated this reaction (ρ = +0.5). The temperature dependence between −32 and −48 °C indicated E_a = 4 ± 0.4 kcal/mol, $\Delta H^{\ddagger}$ = 3.6 ± 0.4 kcal/mol, and $\Delta S^{\ddagger} > -25$ eu. The oxidation of **1**-(*m*-chlorobenzoate) in toluene with peroxyacids afforded an iron(III) porphyrin *N*-oxide (**5**). The reaction required 2 equiv of peroxyacid and afforded 1 mol of a diacylperoxide. The presence of acid discouraged the formation of **5**. Substituent effects in the peroxyacid were the opposite for the formation of **5** (ρ = −0.4) than for the formation of **3**. The results indicated that there are competing homolytic and heterolytic O–O bond cleavage reactions for **2** mediated by iron(III).

Since the discovery of cytochrome P-450 monooxygenase[1] three decades ago, numerous attempts have been made to understand this unique enzyme.[2] The manipulation of molecular oxygen to afford an active oxygen species, the so called "oxenoid" (FeO^{3+}), by utilizing heme iron and reducing equivalents while generally accepted is still poorly understood in chemical terms. The initial steps in the catalytic cycle of cytochrome P-450 have been well established (Scheme I).[2c-e] The reaction sequence involves hydrophobic binding of the substrate close to the heme cofactor in the resting ferric state. Subsequent uptake of a single electron from an associated reductase enzyme and oxygen binding lead

* Author to whom correspondence should be addressed.
† Current address: School of Medicine, Keio University, Tokyo, Japan.

(1) (a) Williams, G. R. unpublished result cited in ref 1b. (b) Klingenberg, M. *Arch. Biochem. Biophys.* **1958**, *75*, 376. (c) Garfinkel, D. *Ibid.* **1958**, *77*, 439.

(2) (a) Brodie, B. B.; Gillette, J. R.; La Du, B. N. *Annu. Rev. Biochem.* **1958**, *27*, 427. (b) Conney, A. H. *Pharmacol. Rev.* **1967**, *19*, 317. (c) *Cytochrome P-450*; Sato, R., Omura, T., Eds.; Kodansha Ltd.: Tokyo, 1978. (d) Estabrook, R. W. In *Methods in Enzymology*; Fleisher, S., Packer, L., Eds.; Academic Press: New York, 1978; Vol. 52, p 43. (e) White, R. E.; Coon, M. J. *Annu. Rev. Biochem.* **1980**, *49*, 315.

0002-7863/88/1510-8443$01.50/0